Gene Editing of Caffeic-O-methyltransferase (COMT1) in the model grass Setaria viridis Improves Biomass Saccharification Without Compromising Plant Growth or Abiotic Stress Tolerance

Fernanda de Oliveira Menezes [a].; Karoline Estefani Duarte [a].; Gabriel Garon Carvalho [b].; Leonardo Dario Gomez [c].; Igor Cesarino [b].; Wagner Rodrigo de Souza [a]*

[a] Federal University of ABC (UFABC), Center for Natural and Human Sciences. Alameda da Universidade, s/n – Anchieta 09606-045, São Bernardo do Campo - SP, Brazil

[b] Department of Botany, Institute of Biosciences, University of São Paulo, Rua do Matão, 27 – Cidade Universitária 73091-7507. São Paulo, Brazil.

[c] Centre for Novel Agricultural Products (CNAP), Department of Biology, University of York, Heslington YO10 5DD, York, UK

Gene Editing of Caffeic-O-methyltransferase (COMT1) in the model grass Setaria viridis Improves Biomass Saccharification Without Compromising Plant Growth or Abiotic Stress Tolerance

Highlights

CRISPR knockout of *COMT1* in *Setaria viridis* markedly enhances biomass digestibility by reducing lignin monomers, without compromising plant growth or salt-stress tolerance.

Genome editing of *COMT1* in *Setaria viridis* reveals unexpected lignin plasticity, reducing S, G, H and tricin units and improving saccharification efficiency without developmental penalties.

Combined thiacidolysis/GC-MS and metabolomics suggests a compensatory mechanism in the lignin portion of the *S. viridis* cell wall.

Abstract

Second-generation bioethanol production is limited by the recalcitrance of lignocellulosic biomass, largely driven by lignin content and composition. Genetic strategies targeting lignin biosynthesis offer a promising alternative to improve biomass digestibility without relying on energy-intensive pretreatments. Here, we used CRISPR/Cas9 editing to disrupt the caffeic-O-methyltransferase gene (*COMT1*) in *Setaria viridis*, a C_4 monocot model related to major bioenergy crops. *COMT1* was selected based on its strong expression in lignifying tissues and its central role in the biosynthesis of syringyl (S) units, guaiacyl (G) units, and the flavone tricin, a non-canonical lignin monomer in grasses. Edited plants showed no visible growth defects, maintaining normal development and salt-stress tolerance. Chemical analyses revealed a drastic reduction in S units and tricin, accompanied by moderate but significant decreases in G and *p*-hydroxyphenyl (H) monomers. Despite these compositional changes, total soluble lignin content was only slightly reduced, suggesting compensatory incorporation of non-canonical monomers. Metabolome analysis of edited plants suggested a redirection of carbon flux towards phenylpropanoid and flavonoid pathways. These modifications resulted in a substantial increase in saccharification efficiency, demonstrating that *COMT1* disruption can enhance biomass digestibility without compromising plant viability. Our findings highlight *COMT1* as a key target for engineering improved feedstocks for bioenergy production.

Keywords

Seteria viridis, *COMT1*, CRISPR/Cas9, lignin biosynthesis, tricin, biomass recalcitrance, saccharification efficiency, cell wall engineering, bioenergy crops

1. Background

As highlighted in the *World Energy Outlook* (U.S. Energy Information Administration, 2021), the energy sector accounts for nearly three-quarters of all anthropogenic greenhouse gas (GHG) emissions worldwide. This alarming statistic underscores the urgent need for transformative changes in how energy is produced and consumed to mitigate climate change and promote long-term ecological resilience effectively. Within this context, the development of sustainable energy systems has gained prominence as a strategic pathway to curb emissions. Among the proposed alternatives, second-generation (E2G) bioethanol derived from lignocellulosic biomass such as agricultural residues has attracted significant international attention as a renewable, low-emission substitute for fossil fuels (Reshmy *et al.*, 2023; Yılbaşı, 2025).

E2G is produced from lignocellulosic biomass derived mainly from agricultural residues such as sugarcane bagasse. The production process begins with a physical and/or chemical pretreatment aimed at reducing biomass recalcitrance by disrupting the lignocellulosic matrix. This step is essential to enhance biomass digestibility, as the rigid cell wall structure limits enzymatic accessibility. Following pretreatment, enzymatic hydrolysis converts structural carbohydrates into fermentable sugars, which are subsequently fermented to ethanol. Improving biomass digestibility remains a major technological bottleneck in E2G production, with a direct impact on process efficiency and economic viability (Liu *et al.*, 2019, Preprint; Kordala *et al.*, 2024, Preprint).

Lignocellulosic biomass primarily comprises three biopolymers that form plant cell walls: cellulose, hemicelluloses, and lignin (Ma *et al.*, 2019, Preprint; Shi *et al.*, 2019). The cellulose polymer forms a scaffold of microfibrils embedded in a matrix of hemicelluloses, which are interlinked with lignin. Lignin, a complex phenolic polymer mainly composed of *p*-hydroxyphenyl (H), guaiacyl (G), and syringyl (S) units, confers mechanical strength to the cell wall, facilitates water transport, and plays key roles in plant defense mechanisms against biotic and abiotic stressors. However, from a bioindustrial perspective, lignin represents a major barrier to biomass deconstruction. Its hydrophobic nature and cross-linking capacity restrict enzymatic access to polysaccharides, thereby reducing sugar release during hydrolysis and compromising fermentation efficiency (Broda *et al.*, 2022, Preprint; Abolore *et al.*, 2024, Preprint).

Although physicochemical pretreatments can partially mitigate biomass recalcitrance, they often require high energy input, increase processing costs, and may produce environmentally harmful byproducts (Basak *et al.*, 2023; Abolore *et al.*, 2024, Preprint). As an alternative, targeted genetic modifications of cell wall components have emerged as a promising strategy to enhance biomass digestibility (Damm *et al.*, 2016, Preprint; Rao and Dixon, 2018, Preprint). Reducing lignin content or altering its composition enhances the release of fermentable sugars from structural carbohydrates, representing a sustainable approach to improving biomass conversion efficiency and reducing second-generation bioethanol production costs (Mosier *et al.*, 2005; Tye *et al.*, 2016, Preprint). However, these genetic modifications often lead to growth penalties, such as reduced biomass yield and increased susceptibility to abiotic stresses, which limit their scalability.

Therefore, optimizing the balance between lignin modification, plant productivity, and stress resilience is essential for advancing the next generation of bioenergy crops (De Vries *et al.*, 2018).

Currently, twelve enzyme families have been identified as key players in the biosynthetic pathway towards canonical lignin monomers (Figure 1). The primary precursor phenylalanine is deaminated into cinnamic acid, which is converted into distinct hydroxycinnamyl alcohols (generally known as monolignols) via hydroxylations/methylations of the aromatic ring and reduction of the propane tail. Multiple routes have been described to contribute to the biosynthesis of monolignols in different plant species, including a tyrosine by-pass via tyrosine ammonia-lyase activity (Barros *et al.*, 2016), the “acid pathway” via bifunctional ascorbate peroxidase activity (Barros *et al.*, 2019), and the highly evolutionarily conserved “shikimate shunt” (Dixon and Barros, 2019, Preprint). The complexity of lignin biosynthesis drastically increases when considering lignin monomers beyond the canonical monolignols, as 49 metabolites have been detected to be incorporated into lignin polymers in different cellular contexts and plant species (Pesquet *et al.*, 2025, Preprint) . Among key lignin biosynthetic enzymes, Caffeic Acid O-Methyltransferase (COMT, E.C. 2.1.1.68) is a *S*-adenosyl-L-methionine-dependent *O*-methyltransferase involved in multiple steps of the pathway. Originally, COMT was thought to catalyze the methylation of caffeic and 5-hydroxyferulic acid, but latter studies demonstrated that this enzyme preferentially methylate 5-hydroxyconiferaldehyde and/or 5-hydroxyconiferyl alcohol to produce sinapaldehyde and/or sinapyl alcohol, respectively (Humphreys J.M and Chapple C, 2002) . Thus, together with Ferulic Acid 5´-Hydroxylase (F5H), COMT constitutes the specific pathway towards the biosynthesis of syringyl lignin units. More recently, COMT-mediated methylation of caffeic acid into ferulic acid was demonstrated to be of great importance for lignification in grasses, being proposed as the most favored route towards G and S units in this group of plants (Barros *et al.*, 2019). Additionally, COMT was demonstrated to play dual roles in the lignin pathway in grasses, as it catalyzes not only the methylation steps within the S-lignin branch but also the methylation steps towards the biosynthesis of the flavone tricin (Eudes *et al.*, 2017) , an authentic lignin monomer in grasses (Lan *et al.*, 2015) . This enzyme also plays an important role in responses to abiotic stresses, such as drought and salinity, through the synthesis of melatonin. COMT catalyzes the conversion of N-acetyl-5-hydroxytryptamine into melatonin, an important regulator of oxidative stress and redox balance in plants, helping to protect cells against damage caused by abiotic stress (Li *et al.*, 2022). Due to its key position in the lignin biosynthetic pathway, the *COMT* gene is considered a suitable target for regulating lignin monomers aimed at reducing biomass recalcitrance.

Studies involving the negative regulation of the *COMT* gene using RNA interference (*RNAi*) techniques in plants of *Brachypodium distachyon* (Ho-Yue-Kuang *et al.*, 2016), *Panicum virgatum* (Wu et al., 2018), and *Hordeum vulgare* (Daly *et al.*, 2019) observed significant changes in lignin composition and biomass digestibility. However, the negative regulation of *COMT* in *Zea mays* and *Sorghum bicolor* plants resulted in negative effects on biomass yield (Miller *et al.*, 1983; Sattler *et al.*, 2010, Preprint). In sugarcane (*Saccharum* sp.), Jung et al. (2012) silenced the COMT gene, addressing biomass digestibility. Although these plants showed increased biomass

125 saccharification, there was also a decrease in productivity. In a more recent study, Kannan et al.
126 (2018) used TALEN-mediated mutagenesis for the knockout of 100 copies/alleles of the *COMT*
127 gene in sugarcane increasing saccharification without compromising biomass.

128 *Setaria viridis* is an emerging monocot model plant for molecular and genetic research. This short,
129 fast-growing, C_4 species has a fully sequenced genome (Bennetzen *et al.*, 2012). It belongs to
130 the *Panicoideae* subfamily, which includes the bioenergy crops *Sorghum bicolor, Zea mays, and*
131 *Saccharum sp.* In a study conducted by Ferreira et al. (2019), six *COMT* genes were identified in
132 the *Setaria viridis* genome. According to this study, the *COMT1 and COMT6* genes showed
133 phylogenetic proximity to the *COMT* genes involved in lignification in *Brachypodium distachyon,*
134 *Zea mays, Oryza sativa,* and *Sorghum bicolor* (Piquemal *et al.*, 2002*a*; Saballos *et al.*, 2008;
135 Koshiba *et al.*, 2013; Trabucco *et al.*, 2013*a*; Ho-Yue-Kuang *et al.*, 2016). Furthermore, it was
136 observed that most of the *COMT* genes showed almost null expression in the elongated internode
137 of *Setaria viridis,* except for *COMT1,* which demonstrated strong and preferential expression in
138 the transition and maturation zones Ferreira et al. (2019) This work shows that *COMT1* is the
139 main candidate gene to play a crucial role in lignification during development in *Setaria viridis.*

140 Here, we demonstrate that CRISPR/Cas9 knockout of the *COMT1* gene in *Setaria viridis*
141 represents a promising strategy to enhance biomass digestibility. The targeted genome editing
142 significantly improved saccharification efficiency without compromising overall plant viability.
143 Notably, despite substantial alterations in lignin composition, the mutant plants maintained normal
144 growth and did not exhibit increased sensitivity to salt stress. These findings underscore the
145 feasibility of engineering lignin pathways without detrimental effects on plant development.

146 2. Materials and methods

147 2.1. Strategies for *COMT1* gene editing in *Setaria viridis* using CRISPR/Cas9

148 The sequence of the target gene, *COMT1* from *Setaria viridis*, was retrieved from the public
149 database Phytozome v13 (https://phytozome-next.jgi.doe.gov/). The genome version used
150 was *Setaria viridis* v4.1, with the corresponding *COMT1* gene ID Sevir. 6G053300.
151 CRISPRPLANT v.2 software (Minkenberg *et al.*, 2019) was utilized to identify the sgRNAs
152 corresponding to the selected gene-editing target, focusing on the region immediately upstream
153 of the PAM sequence (5′-NGG), specific to each gene region to be deleted. The software also
154 enabled the analysis of off-target regions for the selected sgRNAs, and target sites with low
155 probabilities of mis-targeting were chosen for gene editing. The sequences of the sgRNAs for
156 *COMT1* are available in Supplementary Table 1.

157 After identifying the sgRNAs, we proceeded with the construction of vectors for the genetic
158 transformation of *S. viridis*. The selected sequences were cloned into a CRISPR vector (E856;
159 p6i2xoR-UcasW-U6Os4), with codon optimization for monocot species. Cloning was performed
160 by DNA Cloning Service (Hamburg, Germany). The schematic representation of the optimized

161 CRISPR/Cas9 vector is shown in Supplementary Figure 1A, and a schematic representation of
162 the sgRNA target sites in the *COMT1* gene is shown in Supplementary Figure 1B.

163 **2.2. Genetic transformation of *Setaria viridis* and CRISPR/Cas screening**

164 The CRISPR vector was introduced into *Agrobacterium tumefaciens* (strain EAH105α) via heat
165 shock, and genetic transformation of *S. viridis* A10.1 was carried out by co-inoculating
166 embryogenic callus with *A. tumefaciens*, following the protocol adapted from (Martins *et al.*, 2015).
167 Transformed plants were confirmed by PCR using primers specific to the amplification of the *hptII*
168 (244 bp) and *Cas9* (500 bp) genes. Primers used to confirm the transformed events are listed in
169 Supplementary Table 2. To detect insertions or deletions (indels) in the target sites, PCR
170 amplification was performed to generate gene fragments spanning DSB sites (gRNA regions),
171 followed by PCR product purification and Sanger sequencing to validate potential mutations.
172 Chromatograms from sequencing were visualized using BioEdit® software (version 7.2.5). For
173 mutation analysis, we utilized SYNTHEGO software, specifically the ICE (Inference of CRISPR
174 Edits) Analysis tool, as described by (Hsiau *et al.*, 2018, Preprint) (available at
175 https://ice.synthego.com/#/). Samples with R^2 values below 0.8 were excluded due to the lower
176 reliability of the results. In addition to R^2, we also considered the percentages of indels formed,
177 the nature of these indels, and the modifications induced by mutations in the chromatogram. Thus,
178 our analysis included both the percentage of indels and the knockout score.

179 **2.3. Plant material and growth conditions**

180 Independent lines with frameshift mutations were propagated up to the T_2 generation. They were
181 cultivated in a substrate mixed with vermiculite at a 3:1 ratio, in a controlled environment at 28 ±
182 2 °C, with a photoperiod of 16 hours of light and 8 hours of darkness. Irrigation was performed six
183 times a week, maintaining field capacity, while a nutrient solution containing 1 mL of Plant Magic
184 Plus Bio Silicon® per liter of water was applied weekly. The fertilizer composition included 11.7%
185 potassium oxide, 14.3% water-soluble silicon, and 0.05% water-soluble EDTA-chelated iron. Cell
186 wall characterization was conducted with sampling during the senescence phase, when the plants
187 were naturally aging. Plant material (leaves and stems) was processed into powder using a ball
188 mill. Each mutant was treated as an individual biological replicate, and four technical replicates
189 were performed for subsequent analyses

190 **2.4. Cell wall characterization**

191 Independent lines with frameshift mutations were propagated up to the T_2 generation. They were
192 cultivated in a substrate mixed with vermiculite at a 3:1 ratio, in a controlled environment at 28 ±
193 2 °C, with a photoperiod of 16 hours of light and 8 hours of darkness. Irrigation was performed six
194 times a week, maintaining field capacity, while a nutrient solution containing 1 mL of Plant Magic
195 Plus Bio Silicon® per liter of water was applied weekly. The fertilizer composition included 11.7%
196 potassium oxide, 14.3% water-soluble silicon, and 0.05% water-soluble EDTA-chelated iron. Cell
197 wall characterization was conducted with sampling during the senescence phase, when the plants
198 were naturally aging. Plant material (leaves and stems) was processed into powder using a ball

199 mill. Each mutant was treated as an individual biological replicate, and four technical replicates
200 were performed for subsequent analyses.

201 **2.5. Preparation of alcohol insoluble residue (AIR)**

202 Alcohol-insoluble residue (AIR) was prepared as described by Möller et al. (2022), by adding 2
203 mL of water to 100 mg of powdered plant material in a 2 mL Eppendorf tube. The powder was
204 resuspended in the water and shaken by inverting the tube for 30 seconds. The plant material
205 was then pelleted by centrifugation at 4000 *g* for 10 minutes. The supernatant was removed and
206 replaced with 2 mL of 96% ethanol, followed by two additional ethanol washes. The resulting
207 residue was allowed to dry under ambient conditions.

208 **2.6. Lignin quantification by acetyl bromide method**

209 The determination of soluble lignin was carried out by the acetyl bromide method, as described
210 by Liu et al. (2016). Precisely 5 mg of AIR was added to a centrifuge tube with a screw cap, along
211 with 250 µL of acetyl bromide solution (25% acetyl bromide and 75% glacial acetic acid, v/v). The
212 mixture was heated at 50 °C for three hours. After cooling the samples to room temperature, the
213 resulting liquid was transferred to a 5 mL volumetric flask. Next, 1 mL of 2 M NaOH and 175 µL
214 of 0.5 M hydroxylamine hydrochloride (HCl) were added to the reaction. The final volume of the
215 reaction was adjusted precisely to 5 mL using glacial acetic acid. The absorbance of the
216 supernatant was measured on a spectrophotometer at 280 nm. The calculation of the total lignin
217 content in the dry sample was performed using the following formula, where the coefficient used
218 in the calculation was 17.75, specific for grasses (Foster *et al.*, 2010; Dwivedi *et al.*, 2024).
219

220 $$\% \text{ Lignin} = \left(\frac{abs}{coeff\ X\ pathlength}\right) X \left(\frac{total\ volume\ X\ 100\%}{biomass\ weight}\right)$$

221

222 **2.7. Analysis of lignin composition by thioacidolysis method**

223 Lignin composition analysis was also performed using the method described by Chen et al.
224 (2021), with some modifications. Briefly, 1 mL of thioacidolysis reagent (composed of 100 mL of
225 1,4-dioxane, 6.25 mL of boron trifluoride diethyl ether, and 25 mL of ethanethiol, in a v/v ratio) was
226 added to 2.5 mg of AIR. 4,4-Ethylidenebisphenol was added as an internal standard at a final
227 concentration of 12 µg/mL. The reaction was incubated for 4 hours at 100 °C. After cooling, 400
228 µL of the solution was transferred to glass vials, and 190 µL of 0.4 M $NaHCO_3$ were added. The
229 reaction mixture was incubated overnight at 55 °C. The resulting pellet was then homogenized in
230 100 µL of derivatization reagent (1:1 pyridine and BSTFA with 1% TCM v/v) at 55 °C for 30 minutes
231 prior to GC-MS analysis. For tricin analysis, 400 µL of the thioacidolysis reaction was transferred
232 to 1.5 mL tubes, followed by the addition of 190 µL of 0.4 M NaHCO3. This mixture was incubated
233 overnight at 55 °C. The resulting pellet was homogenized in a 1:1 (v/v) methanol:DMSO solution.
234 Samples were sonicated for 10 seconds, centrifuged at 22,000 *g* for 10 minutes, and 100 µL of

235 the supernatant was transferred to vials for HPLC analysis. An Agilent Zorbax Eclipse Plus C18
236 column (2.1 mm × 50 mm, 1.8 µm) was used to separate the compounds. The mobile phases
237 used were: (A) 0.1% formic acid in water (v/v) and (B) 0.1% formic acid in acetonitrile (v/v). The
238 column thermostat was maintained at 30 °C with a solvent flow rate of 0.45 mL/min. The elution
239 gradients were as follows: initially 6% (B) for three minutes, followed by an increase from 6% to
240 95% (B) over 5 minutes. The mobile phase was maintained at 95% (B) for two minutes, followed
241 by a return from 95% to 6% (B) in one minute, and a final phase of two minutes at 6% (B). The
242 total run time was 13 minutes.

243 **2.8. Determination of total *p*-CA and FA by alkaline hydrolysis**

244 The extraction of *p*-coumaric acid (*p*-CA) and ferulic acid (FA) followed the protocol established
245 by Möller et al. (2022). Approximately 10 mg of AIR were incubated with 1M NaOH at 30 °C for
246 12 hours. The reaction was then neutralized with 99% trifluoroacetic acid (TFA) and subjected to
247 a liquid-liquid extraction using 700 µL of butanol. After the evaporation of butanol, the resulting
248 residue was resuspended in a 50% methanol solution and analyzed by high-performance liquid
249 chromatography (HPLC) with UV detection. The injection volume was 10 µL. Component
250 separation was performed using an XBridge BEH Shield RP18 chromatographic column (Waters,
251 186003149) with a porosity of 130 Å, a particle size of 3.5 µm, and dimensions of 1 mm × 100
252 mm. The flow rate was set to 1.23 mL/min, and a binary gradient of 0.1% acetic acid and methanol
253 was applied. The gradient program increased the methanol concentration from 5% to 70% over
254 0–30 minutes, then from 70% to 90% between 30 and 35 minutes and finally returned it to 5%
255 between 35 and 40 minutes. Standard curves were generated using commercial *p*-CA and FA
256 standards (Sigma) over a concentration range of 0.02–3.28 µg/mL for *p*-CA and 0.02–3.88 µg/mL
257 for FA.

258 **2.9. Determination of *p*-CA-arabinose and FA-arabinose by mild acidolysis**

259 The quantification of *p*-coumaric acid and ferulic acid bound to arabinose, *p*-CA-ara and Fa-ara,
260 respectively, was carried out following the protocol described by Lapierre et al. (2018). Briefly, 1
261 mL of the acidolysis reagent (composed of dioxane, methanol, and 2M aqueous hydrochloric acid
262 in a 60:30:10 (v/v/v) ratio) was added to 15 mg of AIR in a screw-cap vial. The incubation was
263 carried out for three hours at 80 °C with shaking at 163 *rpm*. After cooling, the reaction was
264 stopped by the addition of 3 mL of water. The resulting diluted mixture was subjected to two
265 extractions with 1 mL of ethyl acetate, followed by the evaporation of the ethyl acetate and
266 dissolution of the pellet in 100 µL of methanol. The analysis was performed by HPLC, using a
267 binary gradient of 0.1% acetic acid and methanol, with an injection volume of 10 µL. Separation
268 of the sample components was achieved using an XBridge BEH Shield RP18 chromatographic
269 column (Waters - 186003149). The gradient was programmed as follows: for the first 0-60
270 minutes, the methanol concentration was increased from 5% to 65%; from 60-65 minutes, the
271 methanol concentration was increased from 65% to 90%; and from 65-70 minutes, the methanol
272 concentration was returned to 5%.

273

274 **2.10. Monosaccharide analysis**

275 The analysis of the monosaccharide composition of the AIR fraction was performed through the
276 hydrolysis of polysaccharides into monosaccharides. For this, 4 mg of AIR were hydrolyzed in 0.5
277 mL of 2 M trifluoroacetic acid (TFA) for 4 hours at 100 °C. After cooling to room temperature, the
278 solution was completely evaporated using a centrifugal evaporator. The resulting pellet was
279 washed twice with 2-propanol and evaporated. Subsequently, the material was resuspended in
280 200 µL of distilled water, and the suspension was filtered through a 0.45 µm PTFE filter. The
281 analysis was carried out by HPAEC using a Dionex Carbopac PA-10 column with pulsed
282 amperometric detection, as described by Möller et al. (2022) and Wannitikul et al. (2024). The
283 quantification of the isolated monosaccharides was performed using an external calibration curve
284 containing nine monosaccharide standards at concentrations of 250, 500, and 700 µM (glucose,
285 fucose, arabinose, galactose, mannose, rhamnose, xylose, galacturonic acid, glucuronic acid).

286 **2.11. Determination of cellulose content**

287 The quantification of cellulose was carried out according to the methodology outlined by Acevedo
288 et al. (2019). The TFA pellets, obtained as detailed in the previous section, were subjected to a
289 washing procedure with 1.5 mL of water, followed by three additional washes with 1.5 mL of
290 acetone. Subsequently, the samples were air-dried at room temperature overnight. For complete
291 hydrolysis, 90 µL of 72% (w/v) sulfuric acid were added to the dry pellets. Then, 1.89 mL of water
292 was added, and the mixture was heated at 120 °C for 4 hours. The glucose content in the resulting
293 supernatant was determined using the Anthrone colorimetric assay (Morse, 1947) , with a glucose
294 standard curve for quantification. The analysis was performed at a final volume of 1.2 mL, using
295 40 µL of sample and 800 µL of Anthrone (2 mg/mL). The blue color developed after incubation at
296 80 °C for 30 minutes. Standard reactions with glucose concentrations ranging from 0.5 µg/mL to
297 10 µg/mL were included for calibration purposes. The absorbance of the reaction was measured
298 at 620 nm.

299 **2.12. Biomass enzymatic hydrolysis (saccharification)**

300 Enzymatic saccharification was carried out according to the procedures outlined by (Gomez *et*
301 *al.*, 2010). Two types of biomasses were used in the saccharification process: untreated biomass
302 and pretreated biomass. Biomass consisted of whole aerial parts of the plants (leaves + stem).
303 For the pretreatment, 0.5 mL of 500 mM NaOH was added to 100 mg of biomass, and the reaction
304 was heated to 90 °C for 30 minutes with occasional stirring. The material was then decanted to
305 the bottom of the tube. Subsequently, it was washed three times with 1 mL of 25 mM sodium
306 acetate buffer at pH 4.5. For enzymatic saccharification, an enzyme cocktail with a 4:1 ratio of
307 Celluclast to Novozyme 188 was used, where Novozyme 188 acted as a cellulase and was
308 derived from *Aspergillus niger* (both enzymes were obtained from Novozymes, Bagsvaerd,
309 Denmark). Before use, the enzymes were filtered using a Hi-Trap desalting column (GE
310 Healthcare, Little Chalfont, Buckinghamshire, UK). The hydrolysis process was carried out in a

311 25 mM sodium acetate buffer (pH 4.5) at 50 °C for specified time intervals. The determination of
312 sugars released after hydrolysis was performed using a modified version of the method introduced
313 by (Anthon and Barrett, 2002), incorporating 3-methyl-2-benzothiazolinone hydrazone (MBTH).
314 The analysis was conducted in a final volume of 1 mL, with 300 µL of the sample used for the
315 assay. The detection reaction consisted of 0.25 N NaOH, 3 mg/mL MBTH, and 1 mg/mL
316 dithiothreitol (DTT). Color development occurred after incubation at 70 °C for 20 minutes,
317 achieved by adding the oxidizing reagent (0.2% FeNH4(SO4)2, 0.2% sulfamic acid, and 0.1%
318 HCl). Standard reactions with glucose concentrations of 10, 20, 50, and 100 nmol were included
319 for calibration purposes. The absorbance of the reaction was measured at 620 nm. This method
320 was validated to detect a variety of sugars released from the cell wall and demonstrated sensitive
321 detection of several monosaccharides (Gomez *et al.*, 2010).

322 **2.13. Untargeted metabolome profiling**

323 For metabolome analysis, frozen aerial parts were milled with a Grindomix GM200 using
324 precooled stainless-steel jars (Retsch). Metabolites were extracted using 5% acetonitrile, adding
325 a necessary volume to obtain a concentration of 1 mg/mL. The samples were homogenized in
326 vortex for 10 min. at 6720 x *g*. The supernatant was collected and filtered in microfilter PTFE 0.22
327 µm. The filtered samples were injected (5 µL) on a UHPLC system (Waters ACQUITY UPLC)
328 equipped with a HSS T3 column (100 mm by 2.1 mm, 1.8 µm; Waters) and coupled to a Waters
329 Synapt XS qToF (quadrupole time-of-flight) hybrid (Waters) mass spectrometer. A gradient of two
330 buffers (A and B) was utilized: buffer A (0.1 % :formic acid, v/v) and buffer B (99:1:0.1
331 acetonitrile:water:formic acid, pH 3, v/v), as follows: 95% A, 5% B for 3 min, decreased to 50% A
332 and 50% B in 15 min, decreased to 100% B in 18 min and 95% A, 5% B in 20 min , flow rate was
333 0.280 mL per min. LockSpray ion source was used in negative electrospray ionization mode under
334 the following specific conditions: capillary voltage, 2.50 kV; source temperature, 120°C;
335 desolvation gas temperature, 500°C; desolvation gas flow, 1000 L per h; and cone gas flow, 100
336 L/h. The mass range was set from 50 to 1200 Da. For DDA-MSMS, the low mass ramp was
337 ramped between 15 and 50 eV. The peak selection was performed when a peak was > 1% of
338 baseline peak spectra. Data processing was performed with Progenesis QI software version 2.4
339 (Waters). All peaks (mass-to-charge ratio [m/z] features) were integrated in the chromatograms
340 of WT and *SvCOMT* Ev1, Ev2 and Ev3 plants. The following filters were applied to analyze the
341 data: average ion intensity within at least one group >100, P value Student's t-test < 0.001, and
342 fold change >2 or <0.5 compared to the respective control (WT). Peaks that appeared in the blank
343 (30 blank samples) were also excluded from analysis.

344 **2.14. Salt stress assay in hydroponic system**

345 Initially, the seeds were germinated on Petri dishes containing Murashige and Skoog medium with
346 the pH adjusted to 5.8. After germination, the plants were transferred to a hydroponic system and
347 maintained in Hoagland medium (Phytotech Labs, Product ID H353) for 20 days, until the stage
348 just before flowering onset. After the initial growth period, the salinity stress experiment was
349 initiated with three treatments: 0 mM (control), 100 mM, and 250 mM NaCl. The pH of the medium

350 was maintained at 5.8, and the treatment solutions were adjusted according to the specified NaCl
351 concentrations. The growth environment was controlled to maintain a photoperiod of 16 hours of
352 light and 8 hours of darkness, with a constant temperature of 26 °C during both day and night.
353 The nutrient solutions were renewed every 4 days to ensure the maintenance of the desired
354 nutrient and salt concentrations. Plants were collected in quadruplicate after 5 days and 20 days
355 of treatment exposure.

356 **2.15. Determination of relative water content and dry biomass**

357 The relative water content (RWC) of control and stressed plants was determined with 0.2 g of
358 fresh leaves (fresh weight; FW) that were immediately rehydrated in distilled water for 24 h in the
359 dark, when the turgid weight (TW) was recorded. Next, leaves were transferred to an oven set at
360 60 °C and kept until reaching a constant dry weight (DW). Leaf relative water content was
361 calculated using the following equation (Menezes *et al.*, 2020).

362 $\%RWC=100\times(FW-DW)/(TW-DW)$

363 In addition to RWC, the dry biomass of the plants was evaluated after harvesting. Initially, 0.2 g
364 of dry biomass from the aerial part was weighed and then dried in an oven at 60 °C for 24 hours.
365 After this period, the samples were reweighed to determine the final weight.

366 **3. Results**

367 **3.1. CRISPR/Cas9 of *COMT1* editing resulted in plants with different frameshift**
368 **mutations**

369 The strategy for *COMT1* gene knockout was based on the non-homologous end joining (NHEJ)
370 DNA repair pathway, which repairs double-stranded DNA breaks (DSBs) generated by nuclease
371 activity through error-prone ligation. Four sgRNAs were designed to direct the CRISPR/Cas9
372 system to the *COMT1* gene in *Setaria viridis*. The first three (sgRNA1, sgRNA2, and sgRNA3)
373 targeted nucleotides 653–752 within exon 1, a critical coding region essential for gene function,
374 whereas sgRNA4 was designed to target position 1771 in exon 2. This multi-site targeting strategy
375 was intended to maximize knockout efficiency by inducing DSBs at key functional regions of the
376 gene (Supplementary Figure 1B).

377 *Agrobacterium*-mediated transformation generated multiple independent events, confirmed by
378 PCR and Sanger sequencing. Three independent T_2 lines (Ev.1, Ev.2, and Ev.3) carrying
379 frameshift mutations induced by sgRNAs 1, 2, and 3 were selected for further analysis
380 (Supplementary Figure 2 to 4 and Supplementary Table 3). The selected lines exhibited knockout-
381 scores above 70%, as determined by Synthego ICE analysis. This score represents the proportion
382 of indels predicted to cause functional knockouts—specifically frameshift mutations, indels ≥21
383 nucleotides, or edits likely to disrupt protein function. Unlike total indel frequency, which includes
384 all insertions and deletions differing from the wild-type sequence, the knockout-score reflects only
385 those mutations expected to abolish gene function. Scores above 50% are generally associated
386 with biallelic mutations (Synthego, 2018; Conant et al., 2022). Based on these criteria, we

387 selected three homozygous lines with distinct knockout-scores (Ev.1, 91%; Ev.2, 75%; and Ev.3,
388 88%) for subsequent biochemical and phenotypic characterization.

389 3.2. *COMT1* mutants lack the brown midrib phenotype and demonstrate normal 390 growth and development

391 Reduced lignin content and/or altered lignin composition has been frequently associated with the
392 so-called “brown midrib” phenotype in grasses, a characteristic reddish-brown coloration of leaf
393 blade midribs (Sattler *et al.*, 2010, Preprint) . This phenotype has been classically applied to
394 identify and isolate lignin mutants in grasses, given that all mutants arising by either spontaneous
395 or chemical mutagenesis were shown to be associated with loss-of-function of lignin-related
396 genes (Sattler *et al.*, 2010, Preprint; Tang *et al.*, 2014; Li *et al.*, 2015; Tetreault *et al.*, 2021). After
397 generating knockout mutants for *COMT1* in *S. viridis*, we first assessed whether these plants
398 presented the expected brown midrib phenotype. However, the *COMT1* mutants did not exhibit
399 any obvious visible phenotypes. These plants did not show the presence of a brown central vein
400 in the leaves (Figure 2A) nor significant changes in growth patterns (Figure 2B). After senescence,
401 the mutant lines (Ev.1, Ev.2 and Ev.3) were harvested as described in Section 4. Subsequently,
402 we analyzed the effects of the *COMT1* knockout on the cell wall and biomass saccharification of
403 these plants. Since the individual plants exhibited different editing patterns (Supplementary
404 Figures 2, 3 and 4), each mutant was treated as an independent biological replicate, with four
405 technical replicates in the subsequent experiments.

406 3.3. Quantification of lignin content and analysis of its monomeric composition 407 reveal differences in *COMT*-edited plants

408 To investigate the effects of the *COMT1* gene knockout on lignin content and composition, we first
409 quantified the total soluble lignin content in the mutant lines and wild-type plants, following the
410 method described by Liu et al. (2016) . A small but statistically significant reduction in total soluble
411 lignin content was observed in the mutant plants, with a decrease ranging from 1.9% to 3.1%
412 compared to the wild-type plants (Figure 3A). The lignin composition was also analyzed using the
413 thioacidolysis method, as described by Chen et al. (2021). The results of this analysis reveal a
414 significant reduction in the G, S, and H monomers in the edited plants compared to the wild-type
415 (WT) plants. For the G monomer, the reduction ranged from 13.3% to 28.8% (Figure 3B). In the
416 case of the S monomer, reductions were more pronounced, ranging from 81.9% to 76.6% (Figure
417 3C), while the H monomer presented a reduction between 44.1% and 52.5% (Figure 3D).
418 Additionally, tricin, another important component of lignin in grasses, decreased by 44.1% to 51%
419 (Figure 3E).

420 3.4. Total and p-CA-lignin contents are drastically reduced in edited plants

421 Subsequently, the total content of *p*-CA and FA in *Setaria viridis* was measured by HPLC after
422 alkaline hydrolysis in both mutant and wild-type plants. The method used effectively releases
423 nearly all HCAs that are ester-linked, both in arabinoxylan (AX) and lignin (Möller *et al.*, 2022).
424 Our results revealed alterations in the *p*-CA levels in *COMT1* plants. Specifically, as shown in

425 Figure 4A, the total content of *p*-CA decreased by 45% to 51% compared to wild-type plants.
426 Significant changes in FA were also observed in the Ev.2 and Ev.3 lines, with a modest increase
427 of 6% and 4%, respectively. Due to the potential association of ester-linked *p*-CA with both AX
428 and lignin, we employed the methodology described in Lapierre et al. (2018) to extract and
429 quantify HCAs and their conjugates with arabinose (FA-Ara and *p*-CA-Ara) using mild acidolysis.
430 This method allowed us to distinguish between HCAs associated with AX as their arabinose
431 conjugates and those associated with lignin, by subtracting the values of *p*CA-Ara and FA-Ara
432 obtained through mild acidolysis from the values of *p*-CA and FA obtained through alkaline
433 hydrolysis. In this analysis, no significant differences were observed in the levels of *p*-CA and FA
434 esterified to arabinose (*p*-CA-Ara and FA-Ara) in the *COMT1* knockout lines (Ev.1, Ev.2, and Ev.3)
435 compared to the wild-type plants (Figure 4B). However, regarding the *p*-CA bound to lignin, we
436 observed a significant reduction in the *COMT1* knockout plants, with values ranging from 45% to
437 51%. This decrease was also associated with a 6% and 4% increase in lignin-bound FA in lines
438 #2 and #3, respectively (Figure 4C).

439 **3.5. Cellulose content and structural monosaccharide composition did not**
440 **change in mutants compared to wild type plants**

441 The monosaccharide composition of cell wall polymers, determined by high-performance anion-
442 exchange chromatography (HPAEC), showed no significant changes in response to *COMT1* gene
443 knockout (Supplementary Figure 5A). Following this analysis, we evaluated cellulose content,
444 which displayed a slight increase in *COMT1*-knockout plants compared to wild-type controls;
445 however, this difference was not statistically significant (Supplementary Figure 5B). Collectively,
446 these results suggest that the major cell wall modification in the edited plants is associated
447 primarily with alterations in lignin composition.

448 **3.6. The enzymatic hydrolysis of biomass revealed that loss of *COMT1***
449 **increases the saccharification**

450 To assess the impact of *COMT1* knockout on biomass saccharification, enzymatic hydrolysis
451 assays were performed. Biomass from mutant plants exhibited a significant increase in
452 saccharification efficiency, ranging from 34% to 55% relative to wild-type plants, without
453 pretreatment (Figure 5A). Following pretreatment with 500 mM NaOH, saccharification efficiency
454 increased up to threefold in all lines, likely reaching a sugar release plateau. Although *COMT1*
455 knockout plants showed a modest increase in saccharification compared to wild-type, statistical
456 significance was observed only in line #3 (Figure 5B), with no significant differences detected in
457 lines #1 and #2.

458 ***3.7. COMT mutants present altered metabolic flow***

459 Lignin pathway perturbations frequently lead to transcriptional and metabolic reprogramming of
460 the phenylpropanoid pathway, which has been observed for different target genes and plant
461 species (Vanholme *et al.*, 2012; Saleme *et al.*, 2017; Ferreira *et al.*, 2022). Thus, we anticipated
462 that loss of COMT activity results in a redirection of the carbon flux, especially through the

463 phenolic metabolism, given its involvement in different steps of this pathway. To gain insight into
464 the consequences of *COMT1* mutation in the metabolic profile of *S. viridis*, we analyzed
465 acetonitrile-soluble metabolites in aerial parts (leaves + stem) extracts using ultra-high-
466 performance liquid chromatography-mass spectrometry (UHPLC-MS). We were able to detect
467 956 peaks [mass-to-charge ratio (*m/z*) features] with intensities ≥ 1% of the spectra baseline peak
468 (Supplementary Table 4). Then we filtered these peaks based on blank samples, in which all
469 peaks present in the blank samples were removed from analysis when their intensities were
470 comparable to the plant samples, resulting in 160 peaks (Supplementary Table 5). Next, we
471 focused on peaks present in all replicates of at least one sample type, with at least a twofold
472 difference in intensity in *COMT1* mutants compared with controls, resulting in 22 peaks with higher
473 and lower abundances in mutant plants (Table 1).

474 From the 22 peaks differentially abundant in *COMT1* mutants, identified 17 peaks (partially)
475 structurally annotated based on tandem mass spectrometry (MS/MS) fragmentation spectra,
476 using different database analysis. Most were phenolic or flavonoid compounds coupled to sugar
477 moieties, such as hexoses and glucuronic acid, including caffeic acid-*O*-hexoside, kaempferol-3-
478 *O*-caffeoyl glucoside, 2-glucosyloxy-4-methoxycinnamic acid, di-*O*-caffeoyl-hexoside, luteolin-
479 3,7-diglucoside, quercetin-diglucoside, feruloyl-*O*-hexoside and caffeoyl-glucoside. Two
480 compounds are putative G-G dimers coupled to a hexoside moiety, G(8–*O*–4)G-hexoside and
481 G(8–*O*–4) ferulic acid di-(acetylhexoside), increased by two-fold in *COMT* mutants. We also
482 observed one compound involved in phenylpropanoid biosynthesis directly linked to lignin, caffeic
483 acid, increased by 2-fold in *COMT1* mutants. From these 22 peaks, only 4 were decreased in
484 mutant plants, syringaresinol *O*-beta-D-glucoside (decreased by 2-fold), sinapoyl-feruloyl-
485 glucoside (decreased by 6-fold), and 2 unidentified compounds, with *m/z* 577.1576 and 403.1044
486 and retention time 9.55 and 13.18, respectively. These results suggest that disruption of *COMT1*
487 leads to rewiring of the phenolic metabolism in *S. viridis*.

488 3.8. *COMT1* knockout plants did not present altered sensitivity to moderate or 489 severe salinity stress

490 Genetic modifications in the plant cell wall can result in pleiotropic effects, including altered
491 responses to abiotic stresses such as salinity. To determine whether *COMT1* knockout influences
492 plant tolerance to salt stress, a major environmental factor limiting growth and agricultural
493 productivity, we evaluated *COMT1* knockout lines under different NaCl concentrations. Wild-type
494 (WT) plants and knockout lines (Ev.1, Ev.2, and Ev.3) were exposed to 0, 100, and 250 mM NaCl
495 for 5 and 21 days. These NaCL concentrations have been previously shown to cause stress
496 responses in S. viridis (Duarte *et al.*, 2019). Representative phenotypes after 5 days across all
497 treatments are shown in Figures 6A and 6B, while phenotypes after 21 days are presented in
498 Supplementary Figure 6. At 250 mM NaCl, plants of all genotypes failed to survive beyond 9 days
499 (Figure 6C). Conversely, plants submitted to 100 mM NaCl, despite a slight decrease in biomass
500 compared to control (Figure 6B), did not present differences in relative water content (Figure 6A),
501 suggesting a moderate tolerance to salt stress. As shown in Figure 6, this tolerance was not

502 affected by mutations in *COMT1*, as no significant differences in relative water content (RWC) or
503 dry mass were detected between WT and knockout lines after 5 days of 100 mM NaCl (Figures
504 6D and 6E) or 21 days under 100 mM NaCl (Supplementary Figure 6). These results indicate that
505 *COMT1* loss does not impair growth or salt tolerance, as knockout plants maintained RWC levels
506 comparable to WT under saline conditions.

507 **4. Discussion**

508 The conversion efficiency of lignocellulosic biomass into biofuels is inversely correlated with the
509 lignin content in feedstock plants, as demonstrated by Chen and Dixon (2007) and Studer et al.
510 (2011), among many other studies. This correlation arises from the recalcitrance imposed by
511 lignin in the cell wall, which limits enzyme access to structural polysaccharides. Consequently,
512 strategies aimed at reducing lignin content or modifying its structure have been extensively
513 explored to improve biofuel yields from lignocellulosic biomass (Dixon *et al.*, 2001; Fu *et al.*, 2011;
514 Baxter *et al.*, 2014). Different genetic engineering approaches have been employed to decrease
515 lignin content and alter its composition in different species. However, disrupting lignin
516 biosynthesis can lead to undesirable pleiotropic effects, such as reduced mechanical strength
517 and decreased stem rigidity. For instance, in *Arabidopsis thaliana*, mutants with a 50% reduction
518 in lignin content exhibit weaker stems (Jones *et al.*, 2001). Likewise, in tobacco, downregulation
519 of an *O-methyltransferase* reduces lignin levels but also negatively impacts plant growth (Pichon
520 *et al.*, 2006).

521 It is currently known that COMT enzymes play a crucial role in lignin biosynthesis in angiosperms
522 by catalyzing the methylation of the hydroxyl group at the 5-position (5-OH) of intermediates in
523 the phenylpropanoid pathway (Bonawitz and Chapple, 2010, Preprint; Vanholme *et al.*, 2010).
524 This process is essential for the formation of sinapyl alcohol, the main precursor of the S lignin
525 units (Figure 1). Studies indicate that the primary *in vivo* substrates for COMTs are 5-
526 hydroxyconiferaldehyde and 5-hydroxyconiferyl alcohol, intermediates required to produce
527 sinapyl alcohol (Zubieta *et al.*, 2002; Louie *et al.*, 2010; Green *et al.*, 2014). In addition to the
528 methylation of S unit precursors, it is currently accepted that COMT is a bifunctional enzyme in
529 lignin biosynthesis, at least in grasses. In this context, COMT is also responsible for methylation
530 steps that lead to the production of tricin, a member of the flavone subclass of flavonoid
531 compounds, which is incorporated into the lignin polymer via 4-O-β-coupling and is considered
532 the first lignin non-canonical monomer outside the monolignol biosynthetic pathway (Del Río *et*
533 *al.*, 2012; Lan *et al.*, 2016*a*,*b*).

534 In *Setaria viridis*, a study conducted by Ferreira et al. (2019) six *COMT* genes were identified in
535 its genome, all belonging to class II of the *O-methyltransferase* superfamily. These *COMTs* form
536 a distinct phylogenetic group within the monocots, with *COMT1* and *COMT6* showing significant
537 similarity to *COMT* genes involved in lignification in grasses such as *Brachypodium distachyon*,
538 maize, rice, and sorghum. The strong expression of *COMT1* in the transition and maturation
539 zones of the elongated internode in *S. viridis* suggests a central role in lignification, making it an

540 ideal target for genetic manipulation to reduce biomass recalcitrance and improve saccharification
541 efficiency. Therefore, we have chosen *SvCOMT1* as a target for the generation of CRISPR/Cas9
542 mutants in *S. viridis* to disrupt this gene.

543 **The disruption of *COMT1* gene in *Setaria viridis* did not show any visible phenotype**

544 In some C4 grasses, such as *Zea mays* and *Sorghum bicolor*, mutations in genes involved in
545 lignin metabolism, including *COMT*, result in the brown midrib phenotype (*bm* or *bmr*), which is
546 characterized by brown-colored central veins and, often, other parts of the plants. This phenotype
547 is associated with reduced lignin content and increased biomass digestibility (Vignols *et al.*, 1995;
548 Bout and Vermerris, 2003), and it is widely used to identify mutants affected in lignin deposition
549 (Sattler *et al.*, 2010, Preprint). Whereas the majority of the isolated mutants with this phenotype
550 have been characterized as affected in lignin biosynthesis, loss-of-function of genes encoding
551 enzymes that synthesize the methyl donor *S*-adenosyl-L-methionine, used by lignin *O*-
552 methyltransferases, was also shown to result in brown midribs in maize (Tang *et al.*, 2014; Li *et*
553 *al.*, 2015). Additionally, the sorghum *bmr30* mutant has been characterized as disrupted in the
554 tricin biosynthetic gene encoding chalcone isomerase (Tetreault *et al.*, 2021). Until recently, brown
555 midribs have been described only in a few lignin mutants of panicoid C4 grasses such as maize
556 and sorghum, but disruption of some lignin biosynthetic genes in the C3 grass *Brachypodium*
557 *distachyon*, including *COMT*, also resulted in the accumulation of brown pigment in leaf midribs
558 and other lignified tissues (Bouvier D'Yvoire *et al.*, 2013; Trabucco *et al.*, 2013*b*). Conversely, this
559 phenotype has not been found in rice or barley, despite their extensive mutant stocks. Regarding
560 *COMT*, their corresponding mutants in maize and sorghum, as well as their silenced lines in
561 Brachypodium and switchgrass, showed the brown midrib phenotype ('Bout 2003; Piquemal *et*
562 *al.*, 2002*b*; Trabucco *et al.*, 2013*b*; Wu *et al.*, 2019). In addition to the *bmr* phenotype, different
563 studies demonstrated that null *comt* mutant plants presented an abnormal growth (Yu *et al.*,
564 2025), while silenced *COMT* gene plants have reduced lignin content without growth penalties
565 (Vermerris *et al.*, 2007; Saballos *et al.*, 2008; Dien *et al.*, 2009; Fu *et al.*, 2011; Jung *et al.*, 2012,
566 2013; Lam *et al.*, 2019*a*). Here, the *COMT1* edited *S. viridis* plants did not display any visible
567 phenotype, neither the brown midrib trait, nor observable changes in plant growth (Figure 2). In
568 the context of generating optimized feedstock for bioeconomy, the lack of detrimental effects in
569 plant growth and development is a desirable trait. A similar phenotype was found when more than
570 100 *COMT* copies/alleles were gene-edited in sugarcane using TALEN technology (Kannan *et*
571 *al.*, 2018), demonstrating that targeting *COMT* genes using gene editing might be an effective
572 strategy for biomass optimization without yield penalty.

573 ***COMT1* mutants display a drastic reduction of S monomers and a decrease of G, H and**
574 **tricin moieties in the lignin portion of *S. viridis***

575 Our results demonstrated a drastic reduction (from 40 to 80% reduction) in S units and tricin in
576 the AIR of edited *COMT1* plants, while G and H monomers demonstrated less pronounced effects
577 (Figure 4). It is expected that disruption of COMT activity leads to reduction of S units, as the
578 enzyme is mostly involved in the pathway steps that generates S monomers in grasses. The

579 novelty here is that tricin, G and H monomers were also significantly decreased, despite the total
580 soluble lignin content only slightly reduced (Figure 4A). These results may indicate that other
581 steps within the phenylpropanoid/flavonoid pathways might be compensating for lignin
582 biosynthesis through the incorporation of non-canonical monomers, to the extent that normal plant
583 development remains unaffected. The fact that total soluble lignin was only slightly decreased
584 may reinforce the speculation that more soluble, non-canonical monomers, could be incorporated
585 into the lignin.

586 Although the mechanisms underlying lignin homeostasis remain unclear, previous research
587 suggests that plants can preserve lignin deposition by incorporating non-canonical aromatic
588 monomers when canonical monolignols are limited. Reports of flavonoid-derived units,
589 hydroxycinnamate amides, and other atypical phenolics support the view that lignin is more
590 flexible than previously assumed, providing compensatory routes that may stabilize lignin levels
591 despite major pathway disruptions (Ralph et al., 2001b,a; Bonawitz and Chapple, 2010; Vanholme
592 et al., 2010). Also, it is worth mentioning that reduction in S, G and H monolignols may reflect
593 both a global down-regulation of phenylpropanoid flux through feedback inhibition (see Table 1)
594 or/and an altered lignin architecture with increased condensed linkages (C-C linkages instead of
595 β-O-4), which are poorly released by degradative methods.

596 Although there are studies that partially characterize lignin biosynthesis in plants such as
597 *Arabidopsis*, *Oryza sativa*, and *Zea mays*, there are still significant gaps in our understanding of
598 the dynamics of this process in grasses. For example, recent research indicates that many stages
599 of monolignol biosynthesis in grasses do not occur in the same way as in eudicots. In *Arabidopsis*,
600 loss-of-function mutations in genes such as *F5H* and *COM*T lead to a significant reduction in
601 sinapyl lignin units, resulting in a polymer composed solely of G units (Meyer *et al.*, 1998; Goujon
602 *et al.*, 2003). However, in *Oryza sativa*, the loss of function of the *F5H* gene does not result in a
603 complete absence of S units, while in *COMT*-deficient mutants of maize and sorghum, S units are
604 significantly reduced but not completely absent. This suggests that grasses may have alternative
605 pathways to produce these units (Piquemal *et al.*, 2002*a*; Fornalé *et al.*, 2017; Takeda *et al.*,
606 2019). Our results on lignin monomers align with those previously reported in the literature for
607 *Brachypodium distachyon*, *Zea mays*, and *Hordeum vulgare* with *COMT* silencing (Piquemal *et*
608 *al.*, 2002*a*; Barrière *et al.*, 2004; Daly *et al.*, 2019). However, these studies reported that the
609 reduction in S lignin content does not affect G monomers, which contrasts with the findings of the
610 present work. As mentioned above, in *S. viridis* the *COMT1* knockout resulted in significant
611 reductions in G lignin units (ranging from 13.3% to 28.8%), contrary to what was reported in those
612 studies. In alfalfa plants, the negative regulation of *COMT* also caused a decrease in G units and
613 an almost complete loss of S units (Guo *et al.*, 2001). While the formation of G lignin units
614 predominantly depends on CCoAOMT activity, *COMT* may play a secondary role by contributing
615 to the methylation of intermediates feeding into this pathway, such as coniferaldehyde. Thus, the
616 absence of *COMT* could reduce the efficiency of the G unit formation pathway, which explains the
617 decrease in G lignin units observed in our study. Moreover, the reduction in H units observed in
618 *S. viridis* (ranging from 44.1% to 52.5%) can be attributed to the overall modulation of the lignin

619 biosynthetic pathway, where disruption of methylation affects both the accumulation and utilization
620 of precursor monomers. These combined effects confirm that the knockout of the *COMT1* gene
621 not only drastically reduces S units but also impacts the synthesis of other lignin monomers.

622 ***COMT1* mutants demonstrate substantial differences in *p*CA pools**

623 In grasses, lignin and xylan polymers can be substituted with hydroxycinnamic acids (HCAs),
624 such as ferulic acid (FA) and *p*-coumaric acid (*p*-CA). These HCA groups can be esterified or
625 etherified in lignin, playing a crucial role in modulating the structure and properties of the cell wall
626 (Hatfield *et al.*, 2017). In particular, the feruloylation of xylan facilitates the formation of covalent
627 cross-links between xylan chains or between xylan and lignin through the formation of a diferulate
628 (diFA) bridges. This cross-linking process contributes to the rigidity and mechanical strength of
629 the cell wall, as well as affecting biomass digestibility (Hatfield *et al.*, 2017; Terrett and Dupree,
630 2019, Preprint; Feijao *et al.*, 2022).

631 Recent studies suggest that, in grasses, the phenylpropanoid pathway is predominantly directed
632 toward the synthesis of hydroxycinnamic acids (HCAs) (Barros et al. 2022; Karlen et al. 2018;
633 Ralph 2010). This pattern can be attributed to the higher abundance of *p*-coumaric acid (*p*-CA)
634 and ferulic acid (FA) in the cell walls of grasses compared to dicotyledonous species. In this
635 context, *p*-CA plays a crucial role as a precursor in the biosynthesis of various phenylpropanoids
636 and flavonoids (Vogt, 2010) and is commonly conjugated to syringyl (S) and guaiacyl (G) lignin
637 monomers (Peracchi *et al.*, 2024, Preprint). Although the exact function of *p*-CA–lignin conjugates
638 is not fully understood (Hatfield et al. 2017), two main hypotheses have been proposed: (1) *p*-CA
639 may act as a radical transfer agent during the polymerization of S units (Ralph *et al.*, 2004), or (2)
640 *p*-CA-S monomers could terminate polymerization, resulting in a more linear lignin polymer and
641 consequently altering its structural properties (Kishimoto *et al.*, 2005; Hatfield *et al.*, 2017). In
642 addition to its conjugation with S lignin monomers, *p*-coumaric acid (*p*-CA) is also acylated to
643 arabinoxylans in the cell walls of grasses. This process is mediated by BAHD acyltransferases,
644 as demonstrated in species such as *Oryza sativa* (Bartley *et al.*, 2013) and *Setaria viridis* (de
645 Souza *et al.*, 2018; Mota *et al.*, 2021).

646 In the present study, using alkaline hydrolysis and mild acidolysis, we were able to quantify total
647 *p*CA and FA, in addition to *p*CA-Ara and FA-Ara, respectively. Further calculations allowed us to
648 estimate the amount of *p*CA and FA bound to lignin (Figure 4). We observed that there was a
649 large reduction of total *p*CA and *p*CA bound to lignin, while *p*CA-Ara did not show any significant
650 changes in *COMT1* mutants. These results indicate a substantial modulation in the *p*-CA pools,
651 demonstrating that the knockout of *COMT1* directly affects the incorporation of *p*-CA into cell
652 walls, thereby influencing lignin formation and structure. The reduction in total and lignin-bound
653 *p*-CA content observed in our study is consistent with previous reports investigating negative
654 regulation of *COMT* in maize (Pichon *et al.*, 2006) and *Brachypodium distachyon* (Ho-Yue-Kuang
655 *et al.*, 2016), in which decreased levels of *p*-CA and S-type lignin monomers were also observed.
656 Moreover, our results reveal a slight increase in total FA content (ranging from 4% to 6%) in
657 *COMT1* knockout plants. This increase may be associated with compensatory adjustments in the

658 phenylpropanoid biosynthesis caused by disruption of *COMT1*. Evidence of this mechanism has
659 already been reported in genetic modification studies involving the addition of HCAs in *Oryza*
660 *sativa* and *Setaria viridis* (de Souza *et al.*, 2018; Möller *et al.*, 2022). Therefore, we propose that
661 in *S. viridis* ferulic acid biosynthesis is not directly impacted by the knockout of *COMT1*, as its
662 production may proceed via an alternative pathway that bypasses caffeic acid methylation, as
663 suggested by previous studies (Barrière *et al.*, 2004; Chen *et al.*, 2006).

664 **_COMT1_ disruption increased biomass saccharification without altering cell wall**
665 **polysaccharides**

666 *COMT1* knockout revealed no significant changes in the contents of structural polysaccharides
667 (Supplementary Figure 5A). This suggests that, while *COMT* plays a key role in lignin
668 biosynthesis, it does not directly affect cell wall polysaccharides. This result is supported by
669 studies in Arabidopsis and barley, in which loss-of-function of *COMT* did not lead to changes in
670 cellulose or structural carbohydrate content (Lee *et al.*, 2021). Conversely, the amounts of
671 arabinose and xylose released from hemicellulosic polymers were significantly increased in both
672 *COMT* downregulated and knockout rice plants (Lam *et al.*, 2019*b*), demonstrating different
673 results depending on the plant species. As expected for plants with diminished lignin contents,
674 the *COMT1* knockout plants showed a significant increase in biomass saccharification efficiency,
675 ranging from 34% to 55% compared to WT plants, without the necessity for pretreatments (Figure
676 5A). When subjected to pretreatment with 500 mM NaOH, saccharification increased up to
677 threefold, regardless of the genotype, potentially reaching a plateau in sugar release. However,
678 the *COMT1* knockout plants showed only a slight increase in saccharification efficiency compared
679 to the WT plants upon alkaline pretreatment, with no statistically significant differences (Figure
680 5B). The absence of significant differences after pretreatment may be explained by the
681 effectiveness of the pretreatment in breaking down the structural bonds of the cell wall, making
682 the biomass more accessible to enzymes and masking potential differences between the groups.
683 Our results are in line with previous studies that reported a negative correlation between lignin
684 content and the efficiency of hemicellulose enzymatic hydrolysis and fermentation in species such
685 as switchgrass, sugarcane, sorghum, and alfalfa (Chen and Dixon, 2007; Fu *et al.*, 2011; Xu *et*
686 *al.*, 2011; Jung *et al.*, 2012).

687 **Metabolome profiling of _COMT1_ mutants suggests a redirection of carbon flux towards**
688 **phenylpropanoid and flavonoid pathways**

689 Our metabolome analysis demonstrated that, as expected, *COMT1* disruption led to accumulation
690 of caffeic acid, a known (but not preferential) substrate of COMT enzymes (Table 1). However,
691 most tentatively annotated compounds accumulating in *COMT1* mutants were conjugated forms
692 of either flavonoids or phenylpropanoids, such as kaempferol-3-*O*-caffeoyl-glucoside (200-fold
693 increase), 2-glucosyloxy-4-methoxycinnamic acid (4.5-fold increase), caffeoyl-glucoside (44-fold
694 increase) and quercetin-diglucoside (2.6-fold increase). It is not surprising that most of the
695 accumulated metabolites found in edited plants were found as their sugar-conjugated forms,
696 given that several phenylpropanoid derivatives are either cytotoxic and/or bioactive and

697 glycosylation is known to play key roles in modulating phenylpropanoid properties (including
698 solubility, toxicity and bioactivity) and compartmentalization (Rates and Cesarino, 2023, Preprint)
699 . Our results are consistent with some recent studies showing that perturbations of lignin
700 metabolism in grasses lead to the accumulation of glycosylated phenylpropanoids (Barros *et al.*,
701 2022; Ferreira *et al.*, 2022; Oliveira *et al.*, 2025; Priya *et al.*, 2025, Preprint). Importantly, we
702 observed that selgin, the direct precursor of tricin biosynthesis and a known substrate for grass
703 COMTs, is highly accumulated in mutant plants (4.5-fold increase). In addition, luteolin, which is
704 also an intermediate of the tricin pathway and a COMT substrate, also accumulated, but in its
705 conjugated form as luteolin-3',7-diglucoside (2-fold increase). The fact that we did not find in our
706 metabolome many intermediates of the phenylpropanoid pathway suggests that *S. viridis* may
707 have other OMTs involved in lignin biosynthesis through this pathway, or the disruption of *COMT1*
708 is redirecting the carbon flux to flavonoid synthesis. Thus, our results further corroborate that
709 *Setaria viridis* COMT1 play an important role in the synthesis of tricin. The accumulated flavonoids
710 could also be responsible for the resilience of the mutants under salt stress observed in our work.

711 **Salinity stress tolerance is not altered in *COMT1* mutants**

712 Lignin plays a crucial role in plant defense against pathogens and in adaptation to stresses, such
713 as salinity. Given the central role of the *COMT* gene in lignin biosynthesis, we investigated how
714 its knockout affects plant responses to abiotic stresses, particularly salt stress. Soil salinization is
715 a major form of land degradation, characterized by the excessive accumulation of water-soluble
716 salts, especially sodium (Na^+) and chloride (Cl^-) ions (Tian *et al.*, 2021). Several studies have
717 demonstrated that the *COMT* gene regulates plant stress responses, including salinity (Sun *et al.*,
718 2020; Wang *et al.*, 2024), cold (Chang *et al.*, 2021), and drought (Yao *et al.*, 2022).

719 Interestingly, although previous studies have demonstrated that genetic modifications in the
720 *COMT* gene can influence plant responses to salinity, our results show that under moderate
721 salinity levels (100 mM), not only the WT but also genetically modified *Setaria viridis* plants are
722 able to maintain relative water content (RWC) in their tissues (Figure 6), suggesting a moderate
723 tolerance of *S. viridis* to salt stress. Under more severe salinity conditions (250 mM), a reduction
724 of 10.8% in RWC was observed only in line Ev.3, whereas the other edited lines did not show
725 significant changes. Moreover, plant survival was not affected compared to WT, as both WT and
726 *COMT*-knockout plants were able to survive for up to nine days under high salt concentrations.
727 Furthermore, dry biomass measurements (Figure 6) revealed no statistically significant
728 differences between WT and *COMT*-knockout plants at any of the tested NaCl concentrations,
729 both after 5 and 21 days of treatment. These findings suggest that *COMT* gene editing does not
730 significantly affect biomass accumulation under the salinity conditions evaluated.

731 In conclusion, this study highlights the potential of CRISPR/Cas9-mediated knockout of the
732 *COMT1* gene as an effective strategy to alter lignin and improve biomass digestibility in grasses.
733 This has direct implications for enhancing saccharification efficiency and, consequently, biofuel
734 production, without increasing the plants' susceptibility to salt stress. Although the typical *bmr*
735 phenotype was not observed in the mutant lines, the changes in lignin composition and the

significant reduction in S, G, H, and tricin monomers reinforce the role of *COMT1* in modulating lignin structural diversity in grasses. Moreover, the alterations in *p*-coumaric acid (*p*-CA) and ferulic acid (FA) content, combined with metabolomics, suggest the activation of a compensatory mechanism that maintains cell wall structural integrity under both normal and saline conditions. In this context, the application of techniques such as nuclear magnetic resonance (NMR) spectroscopy would be valuable for gaining deeper insights into how *COMT1* knockout-driven modifications affect lignin structure, especially regarding incorporation of non-canonical monomers. Such information could significantly contribute to the rational engineering of plant cell walls without compromising growth. These findings support the notion that genetic manipulation of lignin biosynthetic genes represents a promising approach for optimizing lignocellulosic biomass conversion, with applications in bioenergy and animal nutrition, offering a meaningful contribution toward the development of more efficient and sustainable renewable energy technologies.

Author Contributions

Fernanda de Oliveira Menezes: methodology; investigation; formal analysis; data curation; writing original draft; writing review & editing. **Karoline Estefani Duarte:** supervision; writing review & editing. **Gabriel Garon Carvalho:** formal analysis. **Leonardo Dario Gomez:** methodology; supervision; writing review & editing. **Igor Cesarino:** formal analysis; writing review & editing. **Wagner Rodrigo de Souza:** conceptualization; supervision; project administration; funding acquisition; writing review & editing.

Conflict of Interest

No conflict of interest declared.

Funding Statement

This research was supported by the Fundação de Amparo à Pesquisa do Estado de São Paulo (Fapesp Proc. 2022/04419-5, 2019/26761-4 and 2019/04878-7).

5. References

Abolore RS, Jaiswal S, Jaiswal AK. 2024. Green and sustainable pretreatment methods for cellulose extraction from lignocellulosic biomass and its applications: A review. Elsevier Ltd.

Acevedo A, Simister R, McQueen-Mason SJ, Gómez LD. 2019. Sudangrass, an alternative lignocellulosic feedstock for bioenergy in Argentina. PLoS ONE 14.

Anthon GE, Barrett DM. 2002. Determination of reducing sugars with 3-methyl-2-benzothiazolinonehydrazone. Analytical Biochemistry 305, 287–289.

Barrière Y, Ralph J, Méchin V, Guillaumie S, Grabber JH, Argillier O, Chabbert B, Lapierre C. 2004. Genetic and molecular basis of grass cell wall biosynthesis and degradability. II. Lessons from brown-midrib mutants. Comptes Rendus - Biologies 327, 847–860.

Barros J, Escamilla-Trevino L, Song L, *et al.* 2019. 4-Coumarate 3-hydroxylase in the lignin biosynthesis pathway is a cytosolic ascorbate peroxidase. Nature Communications 10.

Barros J, Serrani-Yarce JC, Chen F, Baxter D, Venables BJ, Dixon RA. 2016. Role of bifunctional ammonia-lyase in grass cell wall biosynthesis. Nature Plants 2.

Barros J, Shrestha HK, Serrani-Yarce JC, Engle NL, Abraham PE, Tschaplinski TJ, Hettich RL, Dixon RA. 2022. Proteomic and metabolic disturbances in lignin-modified Brachypodium distachyon. Plant Cell 34, 3339–3363.

Bartley LE, Peck ML, Kim SR, *et al.* 2013. Overexpression of a BAHD acyltransferase, OsAt10, alters rice cell wall hydroxycinnamic acid content and saccharification. Plant Physiology 161, 1615–1633.

Basak B, Kumar R, Bharadwaj AVSLS, Kim TH, Kim JR, Jang M, Oh SE, Roh HS, Jeon BH. 2023. Advances in physicochemical pretreatment strategies for lignocellulose biomass and their effectiveness in bioconversion for biofuel production. Bioresource Technology 369.

Baxter HL, Mazarei M, Labbe N, *et al.* 2014. Two-year field analysis of reduced recalcitrance transgenic switchgrass. Plant Biotechnology Journal 12, 914–924.

Bennetzen JL, Schmutz J, Wang H, *et al.* 2012. Reference genome sequence of the model plant Setaria. Nature Biotechnology 30, 555–561.

Bonawitz ND, Chapple C. 2010. The genetics of lignin biosynthesis: Connecting genotype to phenotype.

Bout 2003. *in press*.

Bout S, Vermerris W. 2003. A candidate-gene approach to clone the sorghum Brown midrib gene encoding caffeic acid O-methyltransferase. Molecular Genetics and Genomics 269, 205–214.

Bouvier D'Yvoire M, Bouchabke-Coussa O, Voorend W, *et al.* 2013. Disrupting the cinnamyl alcohol dehydrogenase 1 gene (BdCAD1) leads to altered lignification and improved saccharification in Brachypodium distachyon. Plant Journal 73, 496–508.

Broda M, Yelle DJ, Serwańska K. 2022. Bioethanol Production from Lignocellulosic Biomass—Challenges and Solutions. MDPI.

Chang J, Guo Y, Yan J, *et al.* 2021. The role of watermelon caffeic acid O-methyltransferase (ClCOMT1) in melatonin biosynthesis and abiotic stress tolerance. Horticulture Research 8.

Chen F, Dixon RA. 2007. Lignin modification improves fermentable sugar yields for biofuel production. Nature Biotechnology 25, 759–761.

Chen F, Srinivasa Reddy MS, Temple S, Jackson L, Shadle G, Dixon RA. 2006. Multi-site genetic modulation of monolignol biosynthesis suggests new routes for formation of syringyl lignin and wallbound ferulic acid in alfalfa (Medicago sativa L.). Plant Journal 48, 113–124.

Chen F, Zhuo C, Xiao X, Pendergast TH, Devos KM. 2021. A rapid thioacidolysis method for biomass lignin composition and tricin analysis. Biotechnology for Biofuels 14.

Daly P, McClellan C, Maluk M, *et al.* 2019. RNAi-suppression of barley caffeic acid O-methyltransferase modifies lignin despite redundancy in the gene family. Plant Biotechnology Journal 17, 594–607.

Damm T, Commandeur U, Fischer R, Usadel B, Klose H. 2016. Improving the utilization of lignocellulosic biomass by polysaccharide modification. Elsevier Ltd.

Dien BS, Sarath G, Pedersen JF, Sattler SE, Chen H, Funnell-Harris DL, Nichols NN, Cotta MA. 2009. Improved sugar conversion and ethanol yield for forage sorghum (sorghum bicolor L. Moench) lines with reduced lignin contents. Bioenergy Research 2, 153–164.

Dixon RA, Barros J. 2019. Lignin biosynthesis: Old roads revisited and new roads explored. Royal Society Publishing.

Dixon RA, Chen F, Guo D, Parvathi K. 2001. *The biosynthesis of monolignols: a "'metabolic grid'", or independent pathways to guaiacyl and syringyl units?*

Duarte KE, de Souza WR, Santiago TR, Sampaio BL, Ribeiro AP, Cotta MG, da Cunha BADB, Marraccini PRR, Kobayashi AK, Molinari HBC. 2019. Identification and characterization of core abscisic acid (ABA) signaling components and their gene expression profile in response to abiotic stresses in Setaria viridis. Scientific Reports 9.

Dwivedi N, Yamamoto S, Zhao Y, Hou G, Bowling F, Tobimatsu Y, Liu CJ. 2024. Simultaneous suppression of lignin, tricin and wall-bound phenolic biosynthesis via the expression of monolignol 4-O-methyltransferases in rice. Plant Biotechnology Journal 22, 330–346.

Eudes A, Dutta T, Deng K, *et al.* 2017. SbCOMT (Bmr12) is involved in the biosynthesis of tricin-lignin in sorghum. PLoS ONE 12.

Feijao C, Morreel K, Anders N, Tryfona T, Busse-Wicher M, Kotake T, Boerjan W, Dupree P. 2022. Hydroxycinnamic acid-modified xylan side chains and their cross-linking products in rice cell walls are reduced in the Xylosyl arabinosyl substitution of xylan 1 mutant. Plant Journal 109, 1152–1167.

Ferreira SS, Goeminne G, Simoes MS, *et al.* 2022. Transcriptional and metabolic changes associated with internode development and reduced cinnamyl alcohol dehydrogenase activity in sorghum. Journal of Experimental Botany 73, 6307–6333.

Ferreira SS, Simões MS, Carvalho GG, de Lima LGA, Svartman RM de A, Cesarino I. 2019. The lignin toolbox of the model grass Setaria viridis. Plant Molecular Biology 101, 235–255.

Fornalé S, Rencoret J, García-Calvo L, Encina A, Rigau J, Gutiérrez A, Del Río JC, Caparros-Ruiz D. 2017. Changes in cell wall polymers and degradability in maize mutants lacking 30- and 50-o-methyltransferases involved in lignin biosynthesis. Plant and Cell Physiology 58, 240–255.

Foster CE, Martin TM, Pauly M. 2010. Comprehensive compositional analysis of plant cell walls (Lignocellulosic biomass) part I: Lignin. Journal of Visualized Experiments doi: 10.3791/1745.

Fu C, Mielenz JR, Xiao X, *et al.* 2011. Genetic manipulation of lignin reduces recalcitrance and improves ethanol production from switchgrass. Proceedings of the National Academy of Sciences of the United States of America 108, 3803–3808.

Gomez LD, Whitehead C, Barakate A, Halpin C, McQueen-Mason SJ. 2010. Automated saccharification assay for determination of digestibility in plant materials. Biotechnology for Biofuels 3.

Goujon T, Sibout R, Pollet B, *et al.* 2003. *A new Arabidopsis thaliana mutant deficient in the expression of O-methyltransferase impacts lignins and sinapoyl esters*.

Green AR, Lewis KM, Barr JT, Jones JP, Lu F, Ralph J, Vermerris W, Sattler SE, Kang C. 2014. Determination of the structure and catalytic mechanism of sorghum bicolor caffeic acid O-methyltransferase and the structural impact of three brown midrib12 mutations. Plant Physiology 165, 1440–1456.

Guo D, Chen F, Inoue K, Blount JW, Dixon RA. 2001. *Downregulation of Caffeic Acid 3-O-Methyltransferase and Caffeoyl CoA 3-O-Methyltransferase in Transgenic Alfalfa: Impacts on Lignin Structure and Implications for the Biosynthesis of G and S Lignin*.

Hatfield RD, Rancour DM, Marita JM. 2017. Grass cell walls: A story of cross-linking. Frontiers in Plant Science 7.

Ho-Yue-Kuang S, Alvarado C, Antelme S, *et al.* 2016. Mutation in Brachypodium caffeic acid O-methyltransferase 6 alters stem and grain lignins and improves straw saccharification without deteriorating grain quality. Journal of Experimental Botany 67, 227–237.

Hsiau T, Conant D, Rossi N, *et al.* 2018. Inference of CRISPR Edits from Sanger Trace Data. doi: 10.1101/251082. [Preprint].

Humphreys J.M and Chapple C. 2002. Rewriting the lignin roadmap. Current Opinion in Plant Biology 5, 224–229.

Jones L, Ennos AR, Turner SR. 2001. Cloning and characterization of irregular xylem4 (irx4): A severely lignin-deficient mutant of Arabidopsis. Plant Journal 26, 205–216.

Jung JH, Fouad WM, Vermerris W, Gallo M, Altpeter F. 2012. RNAi suppression of lignin biosynthesis in sugarcane reduces recalcitrance for biofuel production from lignocellulosic biomass. Plant Biotechnology Journal 10, 1067–1076.

Jung JH, Vermerris W, Gallo M, Fedenko JR, Erickson JE, Altpeter F. 2013. RNA interference suppression of lignin biosynthesis increases fermentable sugar yields for biofuel production from field-grown sugarcane. Plant Biotechnology Journal 11, 709–716.

Kannan B, Jung JH, Moxley GW, Lee SM, Altpeter F. 2018. TALEN-mediated targeted mutagenesis of more than 100 COMT copies/alleles in highly polyploid sugarcane improves saccharification efficiency without compromising biomass yield. Plant Biotechnology Journal 16, 856–866.

Kishimoto T, Uraki Y, Ubukata M. 2005. Easy synthesis of β-O-4 type lignin related polymers. Organic and Biomolecular Chemistry 3, 1067–1073.

Kordala N, Walter M, Brzozowski B, Lewandowska M. 2024. 2G-biofuel ethanol: an overview of crucial operations, advances and limitations. Springer Science and Business Media Deutschland GmbH.

Koshiba T, Hirose N, Mukai M, Yamamura M, Hattori T, Suzuki S, Sakamoto M, Umezawa T. 2013. Characterization of 5-hydroxyconiferaldehyde O-methyltransferase in Oryza sativa. Plant Biotechnology 30, 157–167.

Lam PY, Tobimatsu Y, Matsumoto N, *et al.* 2019*a*. OsCAldOMT1 is a bifunctional O-methyltransferase involved in the biosynthesis of tricin-lignins in rice cell walls. Scientific Reports 9.

Lam PY, Tobimatsu Y, Matsumoto N, *et al.* 2019*b*. OsCAldOMT1 is a bifunctional O-methyltransferase involved in the biosynthesis of tricin-lignins in rice cell walls. Scientific Reports 9.

Lan W, Lu F, Regner M, Zhu Y, Rencoret J, Ralph SA, Zakai UI, Morreel K, Boerjan W, Ralph J. 2015. Tricin, a flavonoid monomer in monocot lignification. Plant Physiology 167, 1284–1295.

Lan W, Morreel K, Lu F, Rencoret J, del Río JC, Voorend W, Vermerris W, Boerjan W, Ralph J. 2016*a*. Maize tricin-oligolignol metabolites and their implications for monocot lignification. Plant Physiology 171, 810–820.

Lan W, Rencoret J, Lu F, Karlen SD, Smith BG, Harris PJ, del Río JC, Ralph J. 2016*b*. Tricin-lignins: occurrence and quantitation of tricin in relation to phylogeny. Plant Journal 88, 1046–1057.

Lapierre C, Voxeur A, Karlen SD, Helm RF, Ralph J. 2018. Evaluation of Feruloylated and p-Coumaroylated Arabinosyl Units in Grass Arabinoxylans by Acidolysis in Dioxane/Methanol. Journal of Agricultural and Food Chemistry 66, 5418–5424.

Lee JH, Won HJ, Hoang Nguyen Tran P, Lee S mi, Kim HY, Jung JH. 2021. Improving lignocellulosic biofuel production by CRISPR/Cas9-mediated lignin modification in barley. GCB Bioenergy 13, 742–752.

Li L, Hill-Skinner S, Liu S, Beuchle D, Tang HM, Yeh CT, Nettleton D, Schnable PS. 2015. The maize brown midrib4 (bm4) gene encodes a functional folylpolyglutamate synthase. Plant Journal 81, 493–504.

Li R, Yang R, Zheng W, Wu L, Zhang C, Zhang H. 2022. Melatonin Promotes SGT1-Involved Signals to Ameliorate Drought Stress Adaption in Rice. International Journal of Molecular Sciences 23.

Liu B, Gómez LD, Hua C, *et al.* 2016. Linkage mapping of stem saccharification digestibility in rice. PLoS ONE 11.

Liu CG, Xiao Y, Xia XX, Zhao XQ, Peng L, Srinophakun P, Bai FW. 2019. Cellulosic ethanol production: Progress, challenges and strategies for solutions. Elsevier Inc.

Louie G V., Bowman ME, Tu Y, Mouradov A, Spangenberg G, Noel JP. 2010. Structure-function analyses of a caffeic acid O-methyltransferase from perennial ryegrass reveal the molecular basis for substrate preference. Plant Cell 22, 4114–4127.

Ma J, Shi S, Jia X, Xia F, Ma H, Gao J, Xu J. 2019. Advances in catalytic conversion of lignocellulose to chemicals and liquid fuels. Elsevier B.V.

Martins PK, Ribeiro AP, Cunha BADB Da, Kobayashi AK, Molinari HBC. 2015. A simple and highly efficient Agrobacterium-mediated transformation protocol for Setaria viridis. Biotechnology Reports 6, 41–44.

Menezes FO, Carvalho V, Moreira VA, Rigui AP, Gaspar M, Nievola CC. 2020. Juvenile plants of an epiphytic bromeliad exhibit rapid changes in carbohydrate content and antioxidant capacity to cope with water withholding. Theoretical and Experimental Plant Physiology 32, 89–98.

Meyer K, Shirley AM, Cusumano JC, Bell-Lelong DA, Chapple C. 1998. *Lignin monomer composition is determined by the expression of a cytochrome P450-dependent monooxygenase in Arabidopsis*.

Miller JE, Geadelmann JL, Marten GC. 1983. Effect of the Brown Midrib-Allele on Maize Silage Quality and Yield 1 . Crop Science 23, 493–496.

Minkenberg B, Zhang J, Xie K, Yang Y. 2019. CRISPR-PLANT v2: an online resource for highly specific guide RNA spacers based on improved off-target analysis. Blackwell Publishing Ltd.

Möller SR, Lancefield CS, Oates NC, Simister R, Dowle A, Gomez LD, McQueen-Mason SJ. 2022. CRISPR/Cas9 suppression of OsAT10, a rice BAHD acyltransferase, reduces p-coumaric acid incorporation into arabinoxylan without increasing saccharification. Frontiers in Plant Science 13.

Morse EE. 1947. Anthrone in Estimating Low Concentrations of Sucrose. Analytical Chemistry 19, 1012–1013.

Mosier N, Wyman C, Dale B, Elander R, Lee YY, Holtzapple M, Ladisch M. 2005. Features of promising technologies for pretreatment of lignocellulosic biomass. Bioresource Technology 96, 673–686.

Mota TR, de Souza WR, Oliveira DM, *et al.* 2021. Suppression of a BAHD acyltransferase decreases p-coumaroyl on arabinoxylan and improves biomass digestibility in the model grass Setaria viridis. Plant Journal 105, 136–150.

Oliveira DM, Saleme M de LS, Smith RA, *et al.* 2025. CRISPR/Cas9 editing of p-COUMAROYL-CoA:MONOLIGNOL TRANSFERASE 1 in maize alters phenolic metabolism, lignin structure, and lignin-first biomass processing. Trends in Biotechnology 43, 1166–1195.

Peracchi LM, Panahabadi R, Barros-Rios J, Bartley LE, Sanguinet KA. 2024. Grass lignin: biosynthesis, biological roles, and industrial applications. Frontiers Media SA.

Pesquet E, Cesarino I, Kajita S, Pawlowski K. 2025. Physiological roles of lignins – tuning cell wall hygroscopy and biomechanics. John Wiley and Sons Inc doi: 10.1111/nph.70505. [Preprint].

Pichon M, Deswartes C, Gerentes D, Guillaumie S, Lapierre C, Toppan A, Barrière Y, Goffner D. 2006. Variation in lignin and cell wall digestibility in caffeic acid O-methyltransferase down-regulated maize half-sib progenies in field experiments. Molecular Breeding 18, 253–261.

Piquemal J, Chamayou S, Nadaud I, *et al.* 2002*a*. Down-regulation of caffeic acid O-methyltransferase in maize revisited using a transgenic approach. Plant Physiology 130, 1675–1685.

Piquemal J, Chamayou S, Nadaud I, *et al.* 2002*b*. Down-regulation of caffeic acid O-methyltransferase in maize revisited using a transgenic approach. Plant Physiology 130, 1675–1685.

Priya S, Lin H-H, Menon S, *et al.* 2025. Engineered lignin composition in Brachypodium distachyon modulates the root-associated microbiome. doi: 10.1101/2025.07.30.667798. [Preprint].

Ralph J, Bunzel M, Marita JM, Hatfield RD, Lu F, Kim H, Schatz PF, Grabber JH, Steinhart H. 2004. *Peroxidase-dependent cross-linking reactions of p-hydroxycinnamates in plant cell walls*.

Ralph J, Lapierre C, Lu F, Marita JM, Pilate G, Doorsselaere J Van, Boerjan W, Jouanin L. 2001*a*. NMR Evidence for Benzodioxane Structures Resulting from Incorporation of 5-Hydroxyconiferyl Alcohol into Lignins of O-Methyltransferase-Deficient Poplars. doi: 10.1021/jf001042.

Ralph J, Lapierre C, Marita JM, *et al.* 2001*b*. *Elucidation of new structures in lignins of CAD-and COMT-deficient plants by NMR*.

Rao X, Dixon RA. 2018. Current models for transcriptional regulation of secondary cell wall biosynthesis in grasses. Frontiers Media S.A.

Rates A de B, Cesarino I. 2023. Pour some sugar on me: The diverse functions of phenylpropanoid glycosylation. Elsevier GmbH.

Reshmy R, Philip E, Unni R, Paul SA, Sindhu R, Madhavan A, Sirohi R, Pandey A, Binod P. 2023. Bioethanol—A promising alternative fuel for sustainable future. Valorization of Biomass to Bioproducts: Organic Acids and Biofuels. Elsevier, 179–196.

Del Río JC, Rencoret J, Prinsen P, Martínez ÁT, Ralph J, Gutiérrez A. 2012. Structural characterization of wheat straw lignin as revealed by analytical pyrolysis, 2D-NMR, and reductive cleavage methods. Journal of Agricultural and Food Chemistry 60, 5922–5935.

Saballos A, Vermerris W, Rivera L, Ejeta G. 2008. Allelic Association, Chemical Characterization and Saccharification Properties of brown midrib Mutants of Sorghum (Sorghum bicolor (L.) Moench). BioEnergy Research 1, 193–204.

Saleme M de LS, Cesarino I, Vargas L, *et al.* 2017. Silencing CAFFEOYL SHIKIMATE ESTERASE affects lignification and improves saccharification in poplar. Plant Physiology 175, 1040–1057.

Sattler SE, Funnell-Harris DL, Pedersen JF. 2010. Brown midrib mutations and their importance to the utilization of maize, sorghum, and pearl millet lignocellulosic tissues.

Shi N, Liu D, Huang Q, Guo Z, Jiang R, Wang F, Chen Q, Li M, Shen G, Wen F. 2019. Product-oriented decomposition of lignocellulose catalyzed by novel polyoxometalates-ionic liquid mixture. Bioresource Technology 283, 174–183.

de Souza WR, Martins PK, Freeman J, *et al.* 2018. Suppression of a single BAHD gene in Setaria viridis causes large, stable decreases in cell wall feruloylation and increases biomass digestibility. New Phytologist 218, 81–93.

Studer MH, DeMartini JD, Davis MF, Sykes RW, Davison B, Keller M, Tuskan GA, Wyman CE. 2011. Lignin content in natural populus variants affects sugar release. Proceedings of the National Academy of Sciences of the United States of America 108, 6300–6305.

Sun S, Wen D, Yang W, Meng Q, Shi Q, Gong B. 2020. Overexpression of Caffeic Acid O-Methyltransferase 1 (COMT1) Increases Melatonin Level and Salt Stress Tolerance in Tomato Plant. Journal of Plant Growth Regulation 39, 1221–1235.

Takeda Y, Suzuki S, Tobimatsu Y, Osakabe K, Osakabe Y, Ragamustari SK, Sakamoto M, Umezawa T. 2019. Lignin characterization of rice CONIFERALDEHYDE 5-HYDROXYLASE loss-of-function mutants generated with the CRISPR/Cas9 system. Plant Journal 97, 543–554.

Tang HM, Liu S, Hill-Skinner S, Wu W, Reed D, Yeh CT, Nettleton D, Schnable PS. 2014. The maize brown midrib2 (bm2) gene encodes a methylenetetrahydrofolate reductase that contributes to lignin accumulation. Plant Journal 77, 380–392.

Terrett OM, Dupree P. 2019. Covalent interactions between lignin and hemicelluloses in plant secondary cell walls. Elsevier Ltd.

Tetreault HM, Gries T, Liu S, Toy J, Xin Z, Vermerris W, Ralph J, Funnell-Harris DL, Sattler SE. 2021. The Sorghum (Sorghum bicolor) Brown Midrib 30 Gene Encodes a Chalcone Isomerase Required for Cell Wall Lignification. Frontiers in Plant Science 12.

Tian A, Zhao J, Tang B, Zhu D, Fu C, Xiong H. 2021. Study on the Pretreatment of Soil Hyperspectral and Na + Ion Data under Different Degrees of Human Activity Stress by Fractional-Order Derivatives. 13, 3974.

Trabucco GM, Matos DA, Lee SJ, Saathoff AJ, Priest HD, Mockler TC, Sarath G, Hazen SP. 2013*a*. Functional characterization of cinnamyl alcohol dehydrogenase and caffeic acid O-methyltransferase in Brachypodium distachyon. BMC Biotechnology 13.

Trabucco GM, Matos DA, Lee SJ, Saathoff AJ, Priest HD, Mockler TC, Sarath G, Hazen SP. 2013*b*. Functional characterization of cinnamyl alcohol dehydrogenase and caffeic acid O-methyltransferase in Brachypodium distachyon. BMC Biotechnology 13.

Tye YY, Lee KT, Wan Abdullah WN, Leh CP. 2016. The world availability of non-wood lignocellulosic biomass for the production of cellulosic ethanol and potential pretreatments for the enhancement of enzymatic saccharification. Elsevier Ltd.

U.S. Energy Information Administration E. 2021. *Annual Energy Outlook 2021 Narrative*.

Vanholme R, Demedts B, Morreel K, Ralph J, Boerjan W. 2010. Lignin biosynthesis and structure. Plant Physiology 153, 895–905.

Vanholme R, Storme V, Vanholme B, Sundin L, Christensen JH, Goeminne G, Halpin C, Rohde A, Morreel K, Boerjana W. 2012. A systems biology view of responses to lignin biosynthesis perturbations in Arabidopsis. Plant Cell 24, 3506–3529.

Vermerris W, Saballos A, Ejeta G, Mosier NS, Ladisch MR, Carpita NC. 2007. Molecular breeding to enhance ethanol production from corn and sorghum stover. Crop Science.

Vignols F, Rlgau J, Torres MA, Capellades M, Puigdomènech ' P. 1995. *The brown midrib3 (bm3) Mutation in Maize Occurs in the Gene Encoding Caffeic Acid O-Methyltransferase*. American Society of Plant Physiologists.

Vogt T. 2010. Phenylpropanoid biosynthesis. Oxford University Press.

De Vries L, Vanholme R, Van Acker R, De Meester B, Sundin L, Boerjan W. 2018. Stacking of a low-lignin trait with an increas ed guaiacyl and 5-hydroxyguaiacyl unit trait leads to additive and synergistic effects on saccharification efficiency in Arabidopsis thaliana. Biotechnology for Biofuels 11.

Wang H, Chen Z, Luo R, Lei C, Zhang M, Gao A, Pu J, Zhang H. 2024. Caffeic Acid O-Methyltransferase Gene Family in Mango (Mangifera indica L.) with Transcriptional Analysis under Biotic and Abiotic Stresses and the Role of MiCOMT1 in Salt Tolerance. International Journal of Molecular Sciences 25.

Wannitikul P, Dachphun I, Sakulkoo J, Suttangkakul A, Wonnapinij P, Simister R, Gomez LD, Vuttipongchaikij S. 2024. In Vivo Proximity Cross-Linking and Immunoprecipitation of Cell Wall Epitopes Identify Proteins Associated with the Biosynthesis of Matrix Polysaccharides. ACS Omega 9, 31438–31454.

Wu Z, Wang N, Hisano H, Cao Y, Wu F, Liu W, Bao Y, Wang ZY, Fu C. 2019. Simultaneous regulation of F5H in COMT-RNAi transgenic switchgrass alters effects of COMT suppression on syringyl lignin biosynthesis. Plant Biotechnology Journal 17, 836–845.

Xu B, Escamilla-Treviño LL, Sathitsuksanoh N, Shen Z, Shen H, Percival Zhang YH, Dixon RA, Zhao B. 2011. Silencing of 4-coumarate: Coenzyme A ligase in switchgrass leads to reduced lignin content and improved fermentable sugar yields for biofuel production. New Phytologist 192, 611–625.

Yao Z, Zhang X, Liang Y, Zhang J, Xu Y, Chen S, Zhao D. 2022. NtCOMT1 responsible for phytomelatonin biosynthesis confers drought tolerance in Nicotiana tabacum. Phytochemistry 202.

Yılbaşı Z. 2025. Biofuels, E-Fuels, and Waste-Derived Fuels: Advances, Challenges, and Future Directions. Sustainability 17, 6145.

Yu H, Zhang G, Liu J, *et al.* 2025. A functional cascading of lignin modification via repression of caffeic acid O-methyltransferase for bioproduction and anti-oxidation in rice. Journal of Advanced Research doi: 10.1016/j.jare.2025.01.048.

Zubieta C, Kota P, Ferrer JL, Dixon RA, Noel JP. 2002. Structural basis for the modulation of lignin monomer methylation by caffeic acid/5-hydroxyferulic acid 3/5-O-methyltransferase. Plant Cell 14, 1265–1277.

TABLES

Table 1. Differentially accumulated compounds in aerial parts of *SvCOMT1* mutants

Name	RT (min)	Exp. *m/z*	Peak Area±SD				Fold-Change
			WT	Ev.1	Ev.2	Ev.3	
Caffeic acid-O-hexoside	1.29	341.1090	324±117	3572±5689	573±174	426±206	**2.4**
tricetin 3'-O-methyl ether (Selgin)	5.07	315.0719	1261±233	2357±1063	2376±447	1819±322	**4.2**
kaempferol-3-O-caffeoyl-glucoside	6.24	563.1620	ND	232±213	236±89	212±37	**200**
2-Glucosyloxy-4-methoxycinnamic acid	8.23	355.1037	73±22	306±13	519±49	152±20	**4.5**
Di-O-caffeoyl-hexoside	8.86	677.1338	1186±55	2375±105	2769±143	2311±65	**2**
Unknown	8.86	745.1220	99±3	198±5	223±19	201±2	**2**
Luteolin-3',7-diglucoside	8.87	609.1465	8817±332	16666±830	19149±831	16135±663	**2**
Quercetin-diglucoside	8.87	672.1423	344±24	799±41	1102±53	768±65	**2.6**
Unknown	8.87	708.0647	73±2	143±2	172±14	147±14	**2.1**
Feruloyl-O-hexoside	8.98	525.1623	512±59	1323±40	1154±30	923±21	**2.2**
Unknown	9.55	577.1576	214±40	106±2	95±3	115±8	**-2**
G(8–O–4)G-hexoside	9.94	535.1825	1751±338	3879±181	4736±210	2526±279	**2.1**
Flavonoid-diglucuronide	10.12	693.2056	43±18	127±14	184±10	69±5	**3**
Caffeoyl-glucoside	10.17	499.1244	17±13	741±66	1036±13	500±71	**44**
Syringaresinol O-beta-D-glucoside	10.58	579.2041	925±170	424±24	551±9	401±52	**-2**
Caffeic acid	10.64	179.0564	81±34	210±122	179±13	101±13	**2**
Tri-caffeoylquinic acid	11.95	785.1943	762±265	1636±229	2263±530	1660±412	**2.4**
Unknown	11.95	853.1824	62±36	163±18	217±55	165±35	**2.4**
Sinapoyl-feruloyl-glucoside	12.48	583.2194	602±180	104±55	111±10	102±9	**-6**
G(8–O–4) ferulic acid di (acetylhexoside)	12.57	799.2105	1327±508	2235±268	3179±361	2970±450	**2.1**

Dicaffeoyl-hexaric acid	12.58	867.1984	16±8	60±14	138±27	152±37	**7**
Unknown	13.18	403.1044	461±142	174±20	182±52	301±38	**-2**

FIGURE LEGENDS

Figure 1. Lignin biosynthetic pathway in grasses
Current model of lignin biosynthesis encompassing the phenylpropanoid and flavonoid pathways. Preferential carbon flux is indicated by green arrows, while dashed arrows denote unconfirmed steps. The "shikimate shunt" of the phenylpropanoid pathway is highlighted in gray. Solid arrows indicate experimentally confirmed enzymatic steps, and dashed arrows represent suggested conversions. **Phenylpropanoid-related enzymes:** PAL (phenylalanine ammonia-lyase), PTAL (phenylalanine/tyrosine ammonia-lyase), C4H (cinnamate 4-hydroxylase), 4CL (4-hydroxycinnamate:CoA ligase), C3H (4-coumarate 3-hydroxylase/ascorbate peroxidase), CSE (caffeoyl shikimate esterase), HCT (hydroxycinnamoyl-CoA:shikimate/quinate hydroxycinnamoyl transferase), C3'H (4-coumaroyl shikimate 3'-hydroxylase), CCoAOMT (caffeoyl-CoA 3-O-methyltransferase), CCR (cinnamoyl-CoA reductase), F5H (ferulate/coniferaldehyde 5-hydroxylase), COMT (caffeic acid O-methyltransferase), CAD (cinnamyl alcohol dehydrogenase), PMT (p-coumaroyl-CoA:monolignol transferase), FMT (feruloyl-CoA:monolignol transferase). **Flavonoid- and flavone-related enzymes:** CHS (chalcone synthase), CHI (chalcone isomerase), FNSII (flavone synthase II), A3'H/C5'H (apigenin 3'-hydroxylase/chrysoeriol 5'-hydroxylase). The red star marks the intermediates that were altered in *COMT1*-edited plants.

Figure 2. Phenotypes of wild-type (WT) plants and *COMT1* knockout lines.

(A) Leaves of WT plants and *COMT1* knockout lines (Ev.1, Ev.2, and Ev.3). The typical symptoms of *bmr* (brown midrib) mutations, characterized by brown coloration in the central vein, were not observed in the knockout lines. (B) Representative image showing no visible growth differences between WT plants and *COMT1* knockout lines (Ev.1, Ev.2, and Ev.3).

Figure 3. Quantification of lignin content and monomeric composition in wild-type and *COMT1* knockout plants.

(A) Soluble lignin content determined by the acetyl bromide method, and levels of (B) guaiacyl (G), (C) syringyl (S), (D) p-hydroxyphenyl (H), and (E) tricin monomers in alcohol-insoluble residue (AIR) extracts. Lignin content and monomeric composition were analyzed in wild-type (WT) plants and in three independent *COMT1* knockout lines (Ev.1, Ev.2, and Ev.3). Values are expressed as µg/mg AIR and represent means ± SEM (n = 4). Statistical differences between WT and knockout lines were assessed using one-way ANOVA followed by Tukey's post hoc test (*P < 0.05; **P < 0.01; ***P < 0.001; ***P < 0.0001; n.s., not significant).

Figure 4. Determination of hydroxycinnamic acid (HCA) content.

(A) Total HCA content, (B) HCA content linked to arabinose, and (C) HCA content bound to lignin. The analysis was performed on wild-type (WT) plants and *COMT1* knockout lines (Ev.1, Ev.2, and Ev.3). Values were obtained by alkaline hydrolysis per mg of the AIR (Alcohol-Insoluble Residue)

fraction and are expressed as means ± SEM (n = 4). Statistical significance between *COMT1* knockout lines and WT was assessed by one-way ANOVA followed by Tukey's post hoc test. Significance levels: *P < 0.05; **P < 0.01; ***P < 0.001; ****P < 0.0001; n.s., not significant

Figure *5*. Biomass saccharification analysis.

The analysis was conducted on wild-type (WT) plants and *COMT1* knockout lines (Ev.1, Ev.2, and Ev.3) using untreated biomass (A) and biomass treated with 500 mM NaOH (B). Values are expressed as nmol of glucose released per mg of AIR (alcohol-insoluble residue), and data are presented as means ± SEM (n = 4). Statistical significance between *COMT1* knockout lines and WT was assessed by one-way ANOVA followed by Tukey's post hoc test. Significance levels: *P < 0.05; **P < 0.01; ***P < 0.001; ****P < 0.0001; n.s., not significant.

Figure 6. Responses of Relative Water Content and Dry Mass in Wild-Type and *COMT1* Knockout Plants to 5-Day NaCl Treatments

(A–B) Representative phenotypes after 5 days of exposure to 0, 100, and 250 mM NaCl. (C) Survival of plants exposed to 250 mM NaCl, showing that all genotypes failed to survive beyond 9 days. (D–E) Relative water content (RWC) and dry mass after 5 days under the indicated NaCl concentrations. Values are presented as means ± SEM (n = 4). Statistical significance relative to WT was determined by one-way ANOVA followed by Tukey's post hoc test ($p \leq 0.05$); n.s., not significant.

Figure 1

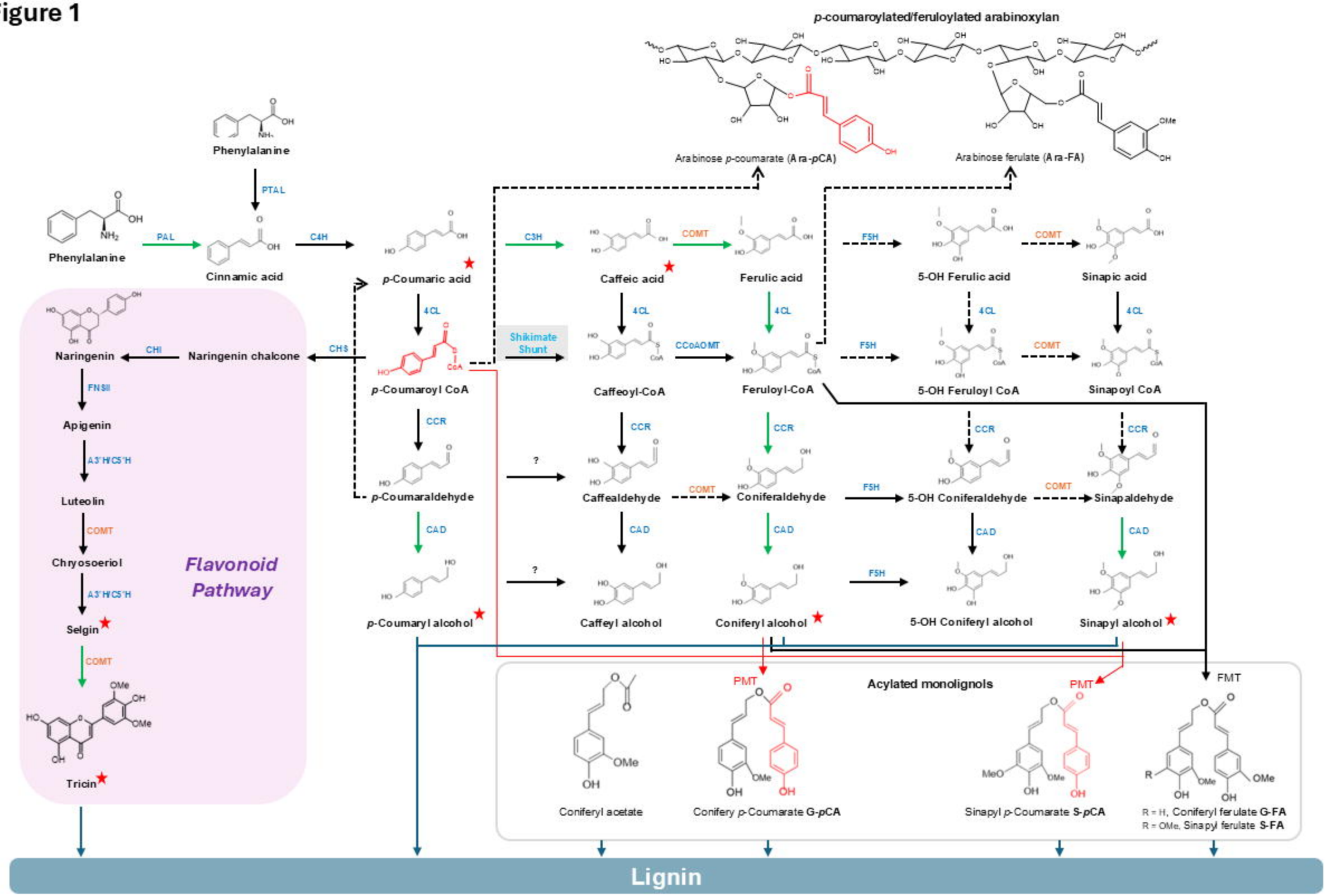
p-coumaroylated/feruloylated arabinoxylan
Arabinose p-coumarate (Ara-pCA)
Arabinose ferulate (Ara-FA)
Phenylalanine
PTAL
Phenylalanine
PAL
Cinnamic acid
C4H
p-Coumaric acid
C3H
Caffeic acid
COMT
Ferulic acid
F5H
5-OH Ferulic acid
COMT
Sinapic acid
4CL
p-Coumaroyl CoA
Shikimate Shunt
Caffeoyl-CoA
CCoAOMT
Feruloyl-CoA
5-OH Feruloyl CoA
Sinapoyl CoA
CHS
Naringenin chalcone
CHI
Naringenin
FNSII
Apigenin
A3'H/C5'H
Luteolin
COMT
Chryosoeriol
A3'H/C5'H
Selgin
COMT
Tricin
Flavonoid Pathway
CCR
p-Coumaraldehyde
?
Caffealdehyde
COMT
Coniferaldehyde
F5H
5-OH Coniferaldehyde
COMT
Sinapaldehyde
CAD
p-Coumaryl alcohol
Caffeyl alcohol
Coniferyl alcohol
5-OH Coniferyl alcohol
Sinapyl alcohol
PMT
FMT
Acylated monolignols
Coniferyl acetate
Conifery p-Coumarate G-pCA
Sinapyl p-Coumarate S-pCA
R = H, Coniferyl ferulate G-FA
R = OMe, Sinapyl ferulate S-FA
Lignin

Figure 2

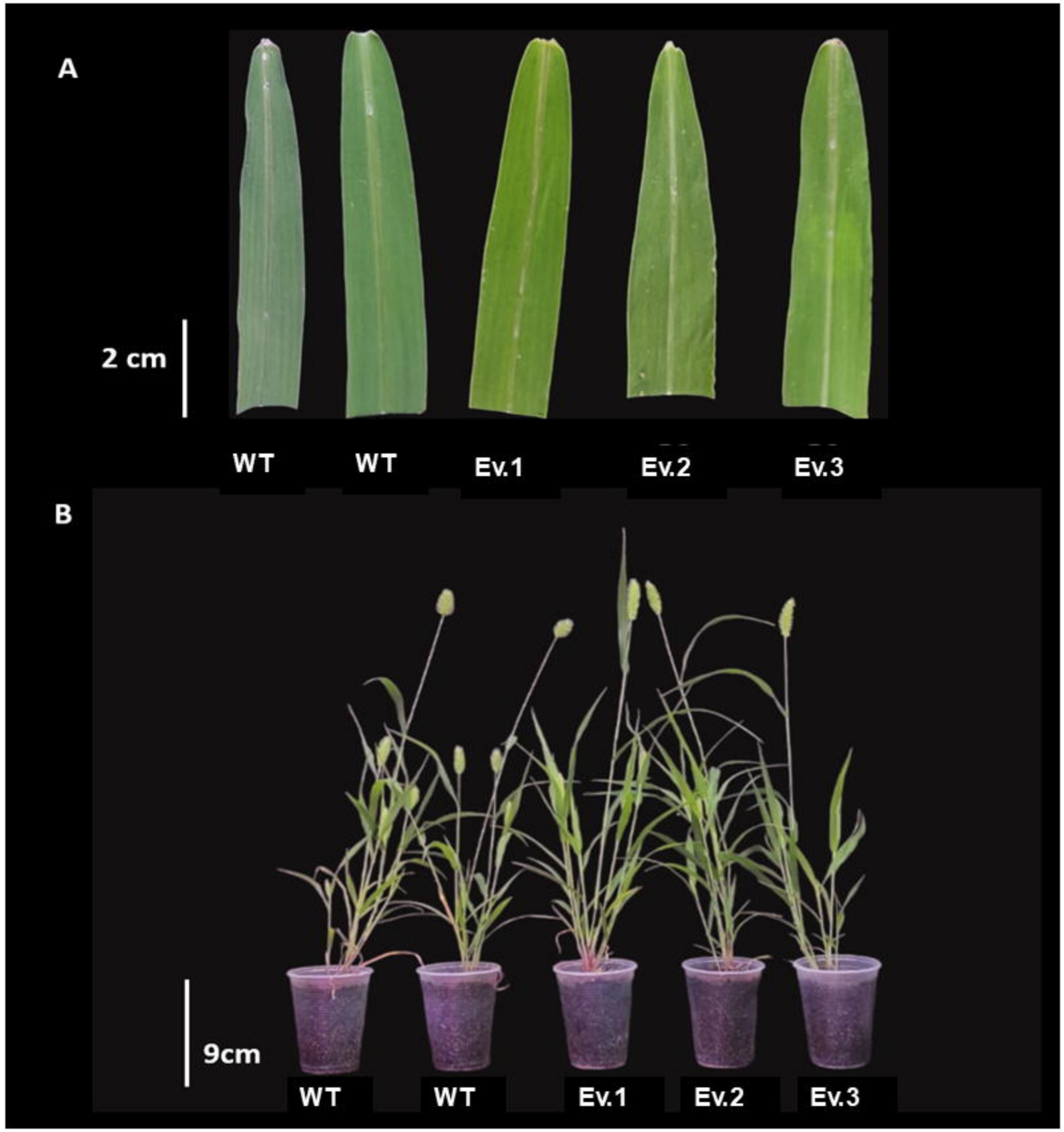

Figure 3

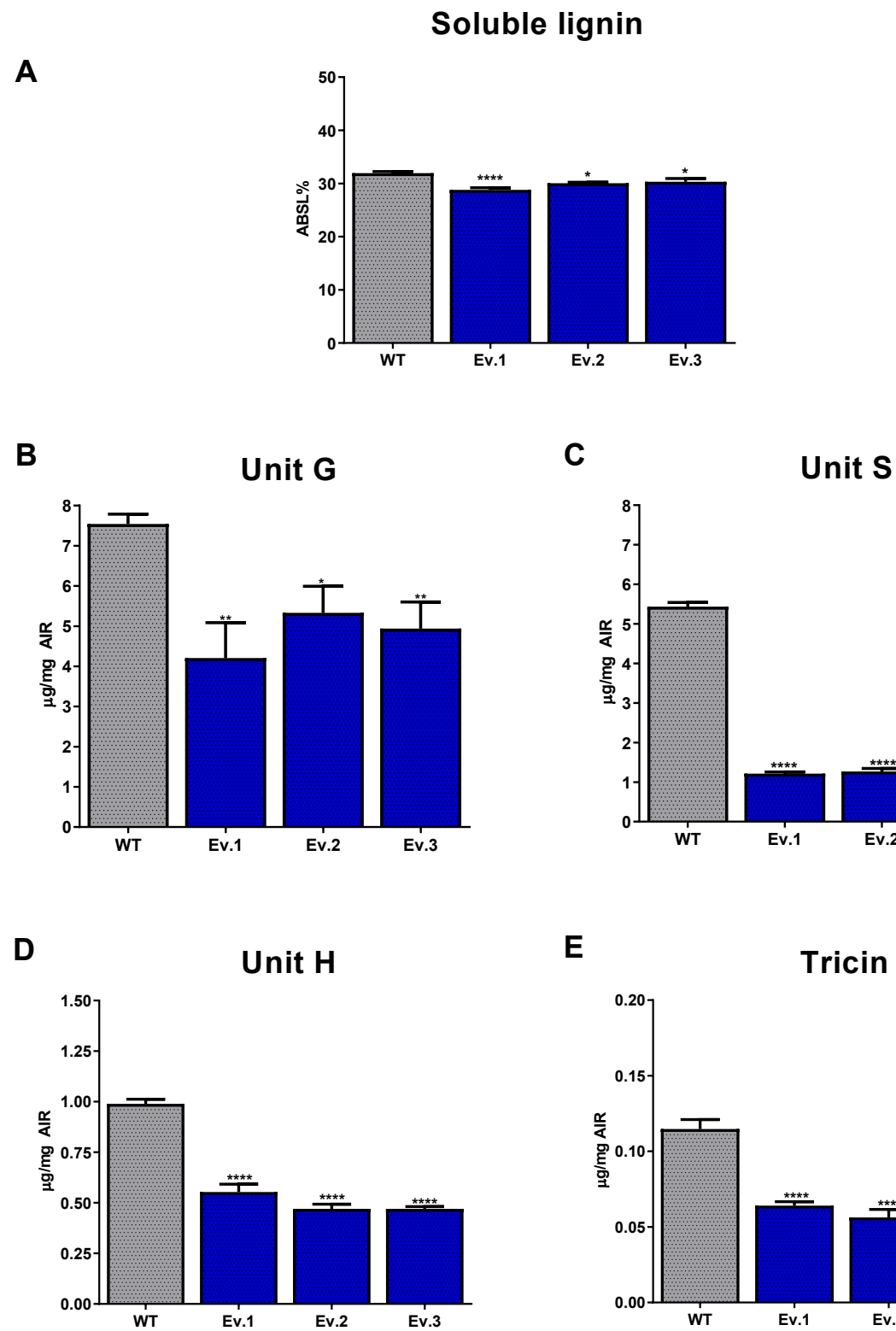
A
Soluble lignin
ABSL%
50
40
30
20
10
0
****
*
*
WT
Ev.1
Ev.2
Ev.3
B
Unit G
µg/mg AIR
8
7
6
5
4
3
2
1
0
**
*
**
WT
Ev.1
Ev.2
Ev.3
C
Unit S
µg/mg AIR
8
7
6
5
4
3
2
1
0
****
****
****
WT
Ev.1
Ev.2
Ev.3
D
Unit H
µg/mg AIR
1.50
1.25
1.00
0.75
0.50
0.25
0.00
****
****
****
WT
Ev.1
Ev.2
Ev.3
E
Tricin
µg/mg AIR
0.20
0.15
0.10
0.05
0.00
****
****
****
WT
Ev.1
Ev.2
Ev.3

Figure 4

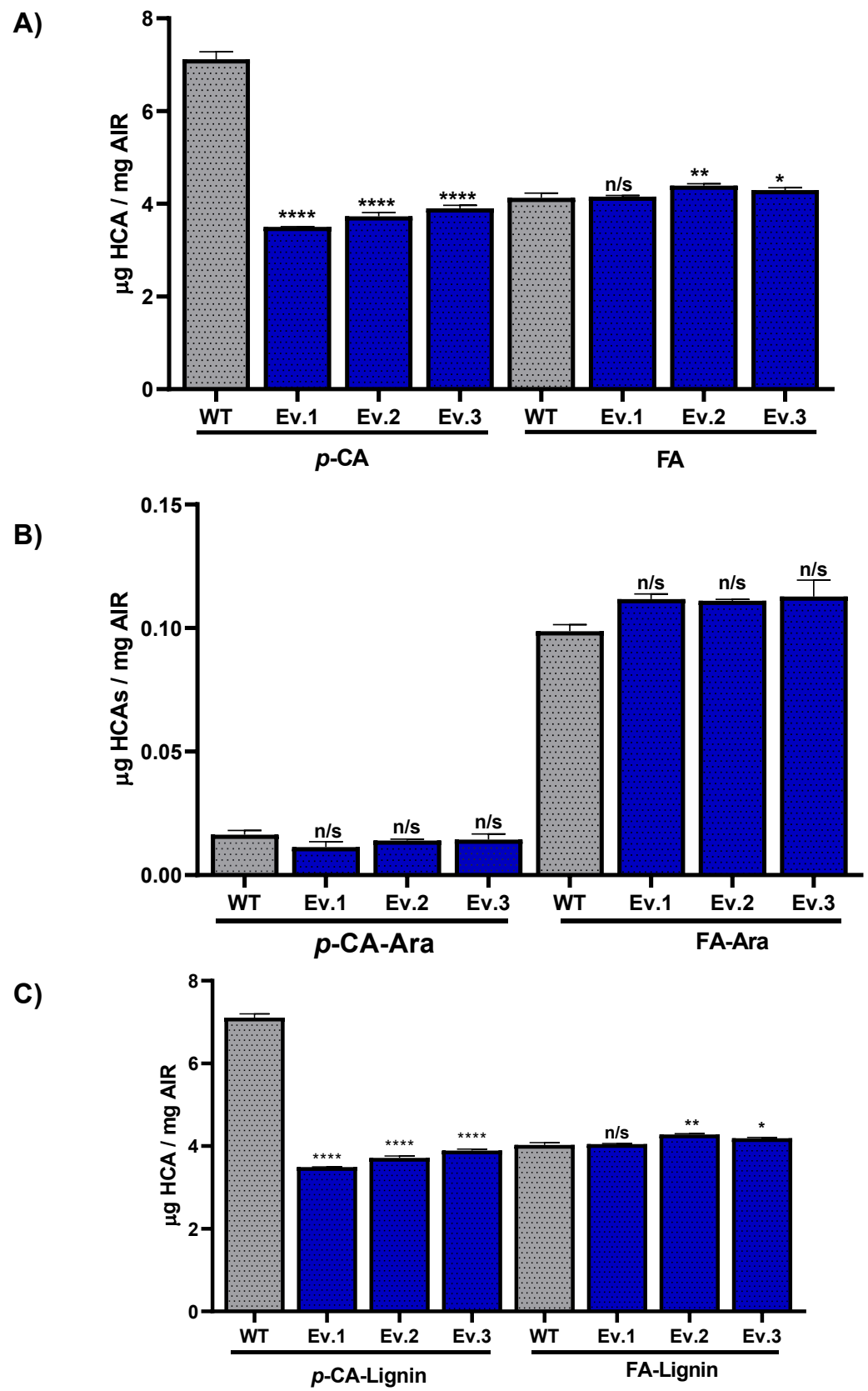
A)
µg HCA / mg AIR
8
6
4
2
0
****
****
****
n/s
**
*
WT
Ev.1
Ev.2
Ev.3
WT
Ev.1
Ev.2
Ev.3
p-CA
FA
B)
µg HCAs / mg AIR
0.15
0.10
0.05
0.00
n/s
n/s
n/s
n/s
n/s
n/s
WT
Ev.1
Ev.2
Ev.3
WT
Ev.1
Ev.2
Ev.3
p-CA-Ara
FA-Ara
C)
µg HCA / mg AIR
8
6
4
2
0
****
****
****
n/s
**
*
WT
Ev.1
Ev.2
Ev.3
WT
Ev.1
Ev.2
Ev.3
p-CA-Lignin
FA-Lignin

Figure 5

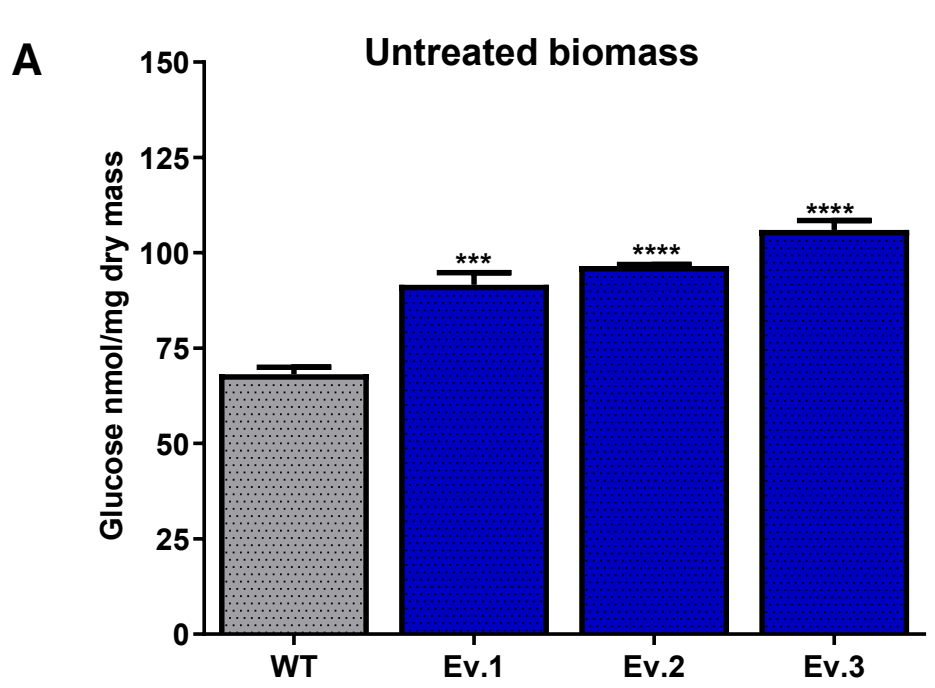
A
Untreated biomass
Glucose nmol/mg dry mass
150
125
100
75
50
25
0
***
****
****
WT
Ev.1
Ev.2
Ev.3

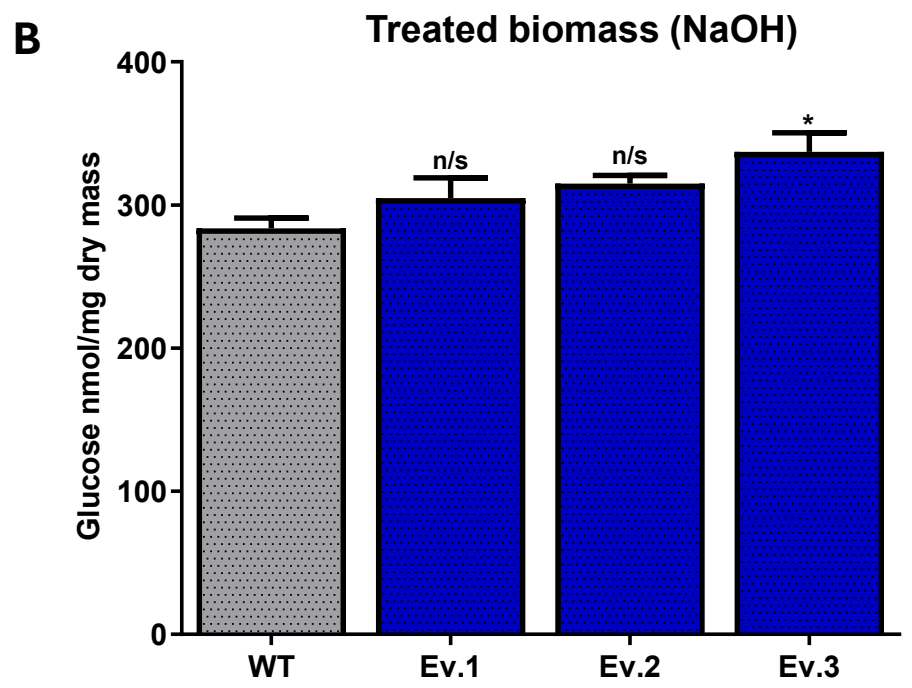
B
Treated biomass (NaOH)
Glucose nmol/mg dry mass
400
300
200
100
0
n/s
n/s
*
WT
Ev.1
Ev.2
Ev.3

Figure 6

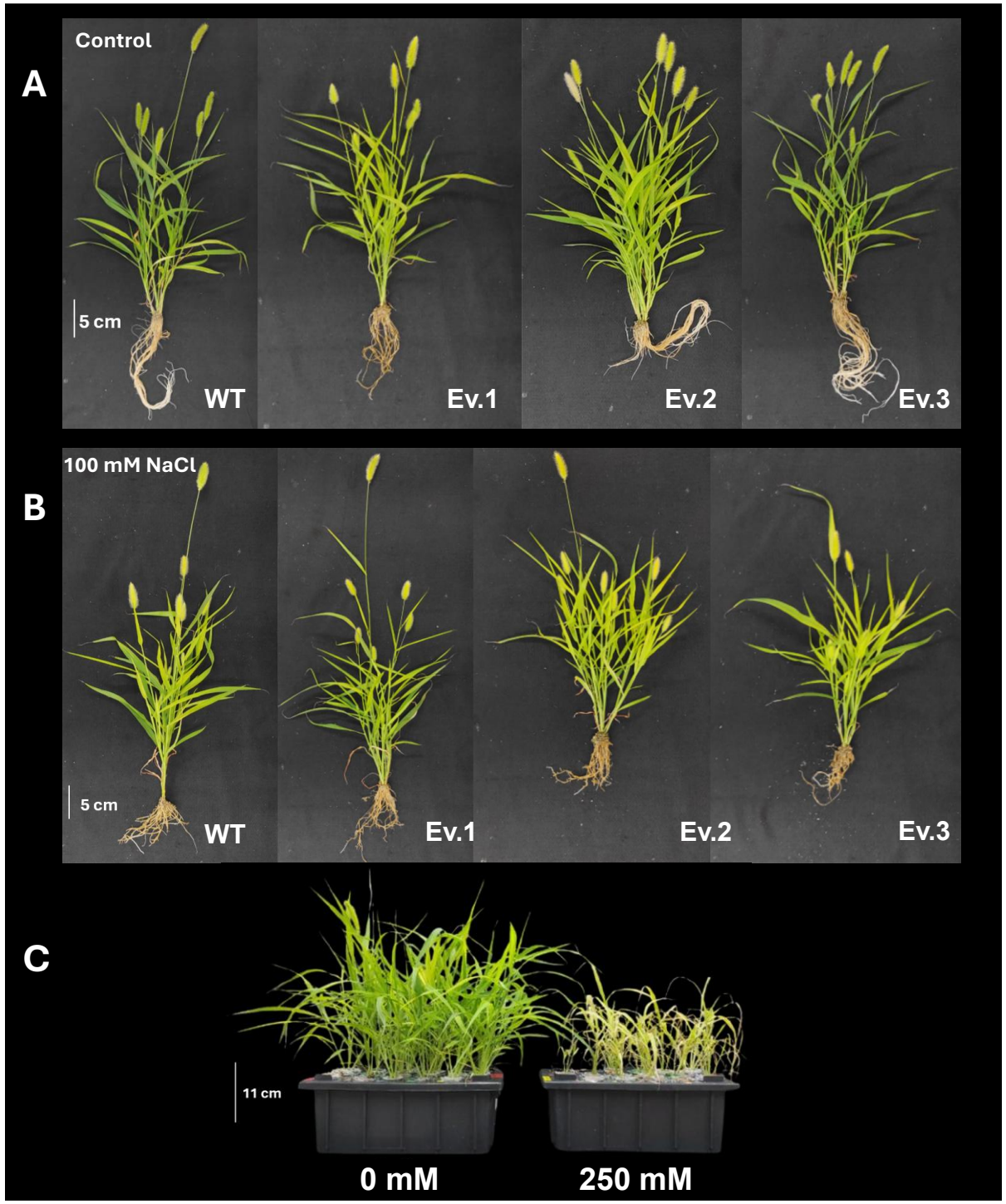
A
Control
5 cm
WT
Ev.1
Ev.2
Ev.3
B
100 mM NaCl
5 cm
WT
Ev.1
Ev.2
Ev.3
C
11 cm
0 mM
250 mM

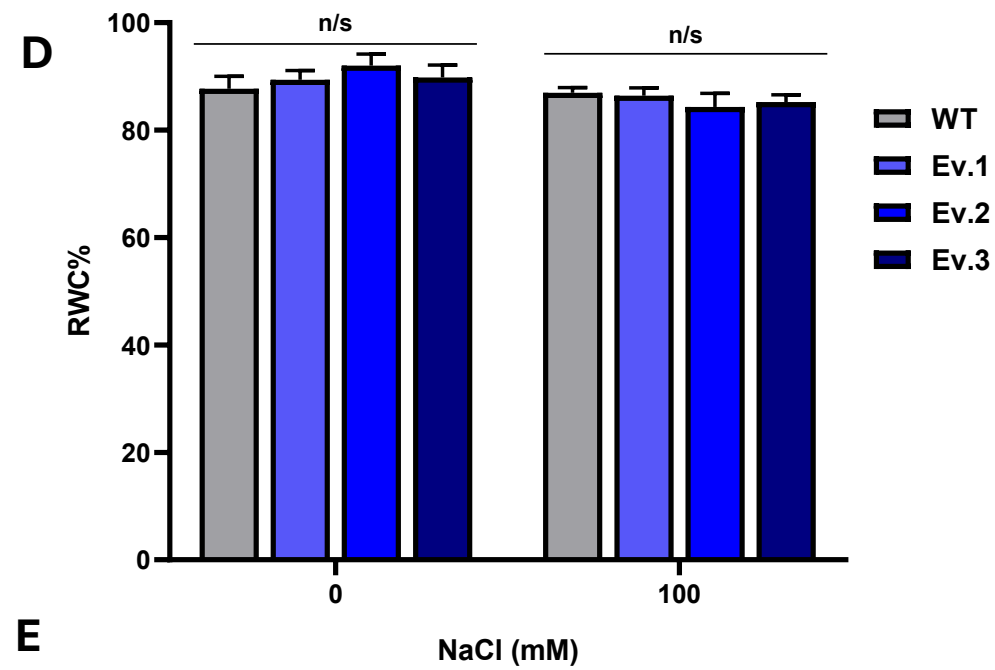
D
RWC%
100
80
60
40
20
0
n/s
n/s
0
100
NaCl (mM)
WT
Ev.1
Ev.2
Ev.3

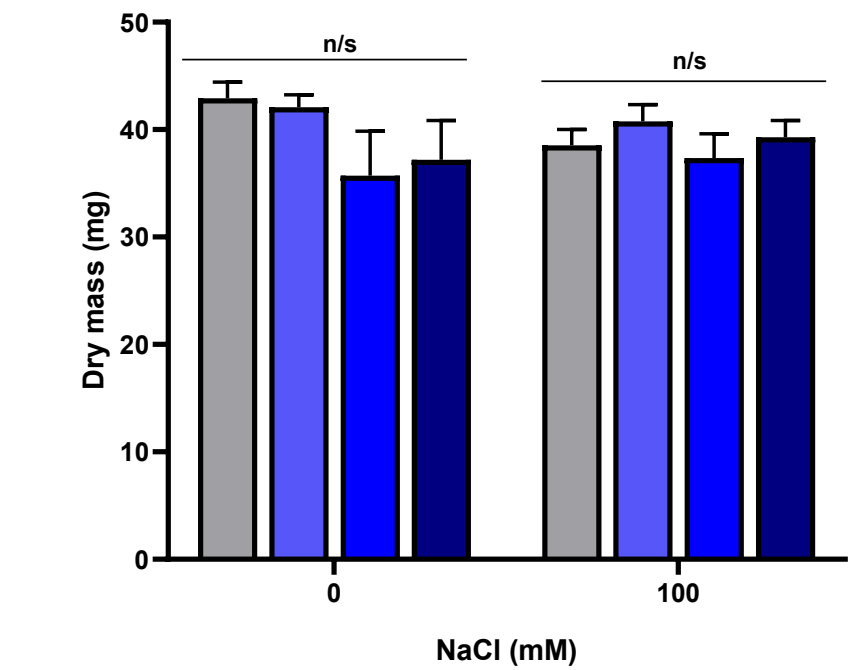
E
Dry mass (mg)
50
40
30
20
10
0
n/s
n/s
0
100
NaCl (mM)

Figure S1

A

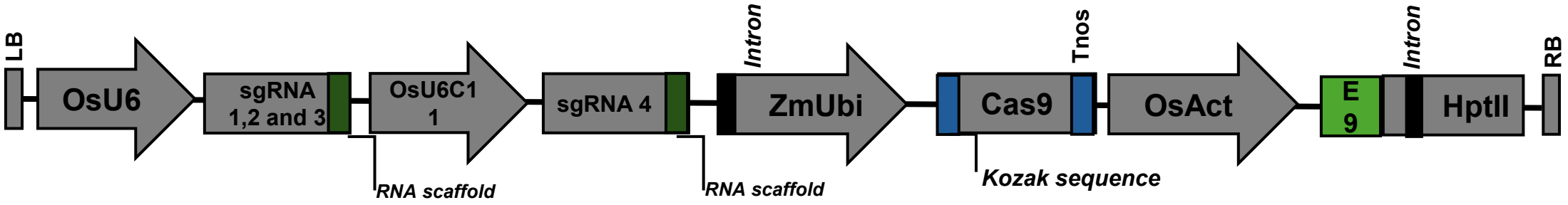
LB
OsU6
sgRNA 1,2 and 3
OsU6C1 1
RNA scaffold
sgRNA 4
RNA scaffold
Intron
ZmUbi
Tnos
Cas9
Kozak sequence
OsAct
E 9
Intron
HptII
RB

B

COMT1
5'
3'
Exon 1
Exon 2
0bp
653bp sgRNA1
689bp sgRNA2
752bp sgRNA3
1500bp
1771bp sgRNA4
2500bp
Éxon
Upstream/downstream
Intron

Figure S2

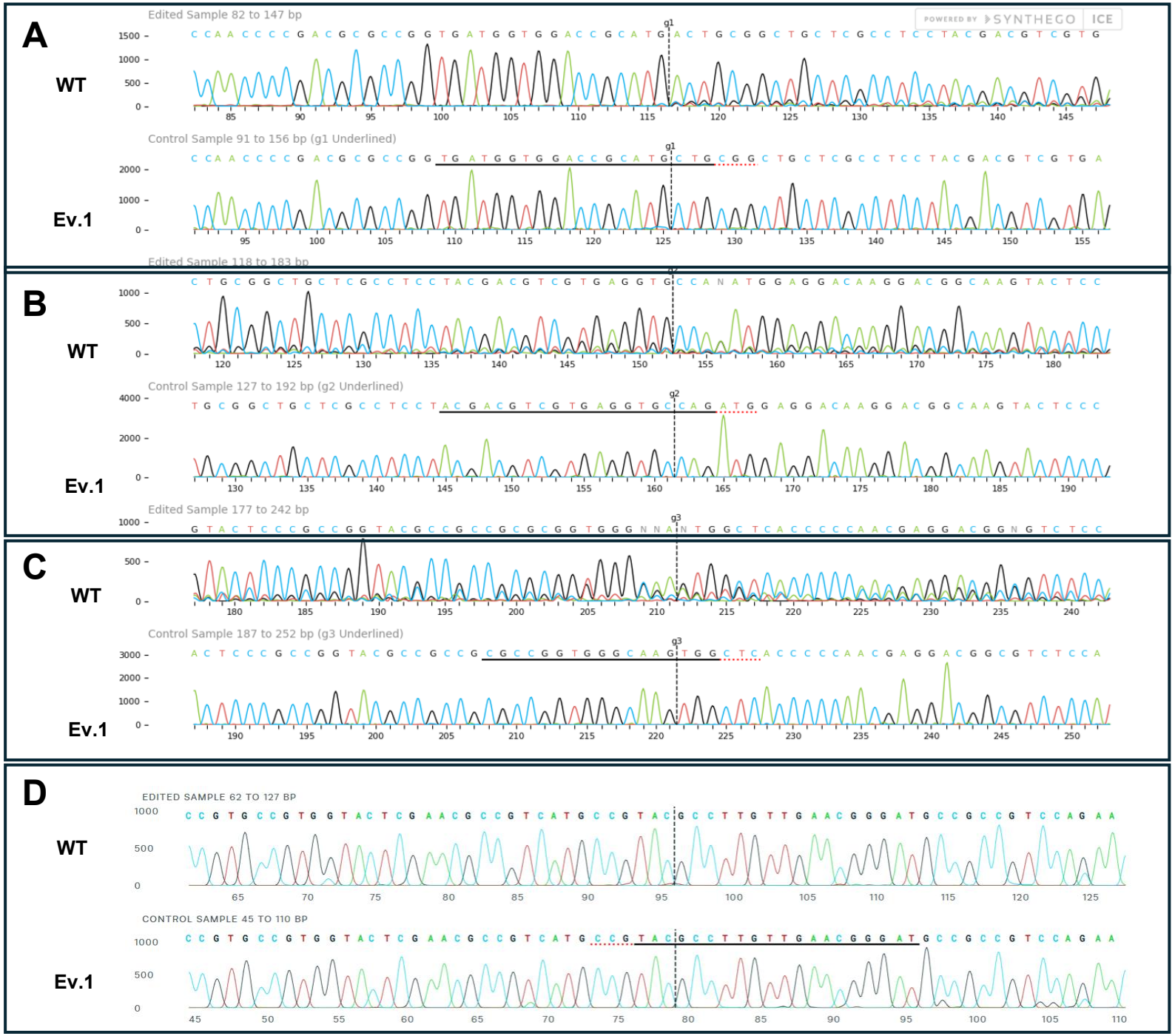
A
WT
Edited Sample 82 to 147 bp
POWERED BY SYNTHEGO ICE
Ev.1
Control Sample 91 to 156 bp (g1 Underlined)
B
WT
Edited Sample 118 to 183 bp
Ev.1
Control Sample 127 to 192 bp (g2 Underlined)
Edited Sample 177 to 242 bp
C
WT
Ev.1
Control Sample 187 to 252 bp (g3 Underlined)
D
WT
EDITED SAMPLE 62 TO 127 BP
Ev.1
CONTROL SAMPLE 45 TO 110 BP

Figure S3

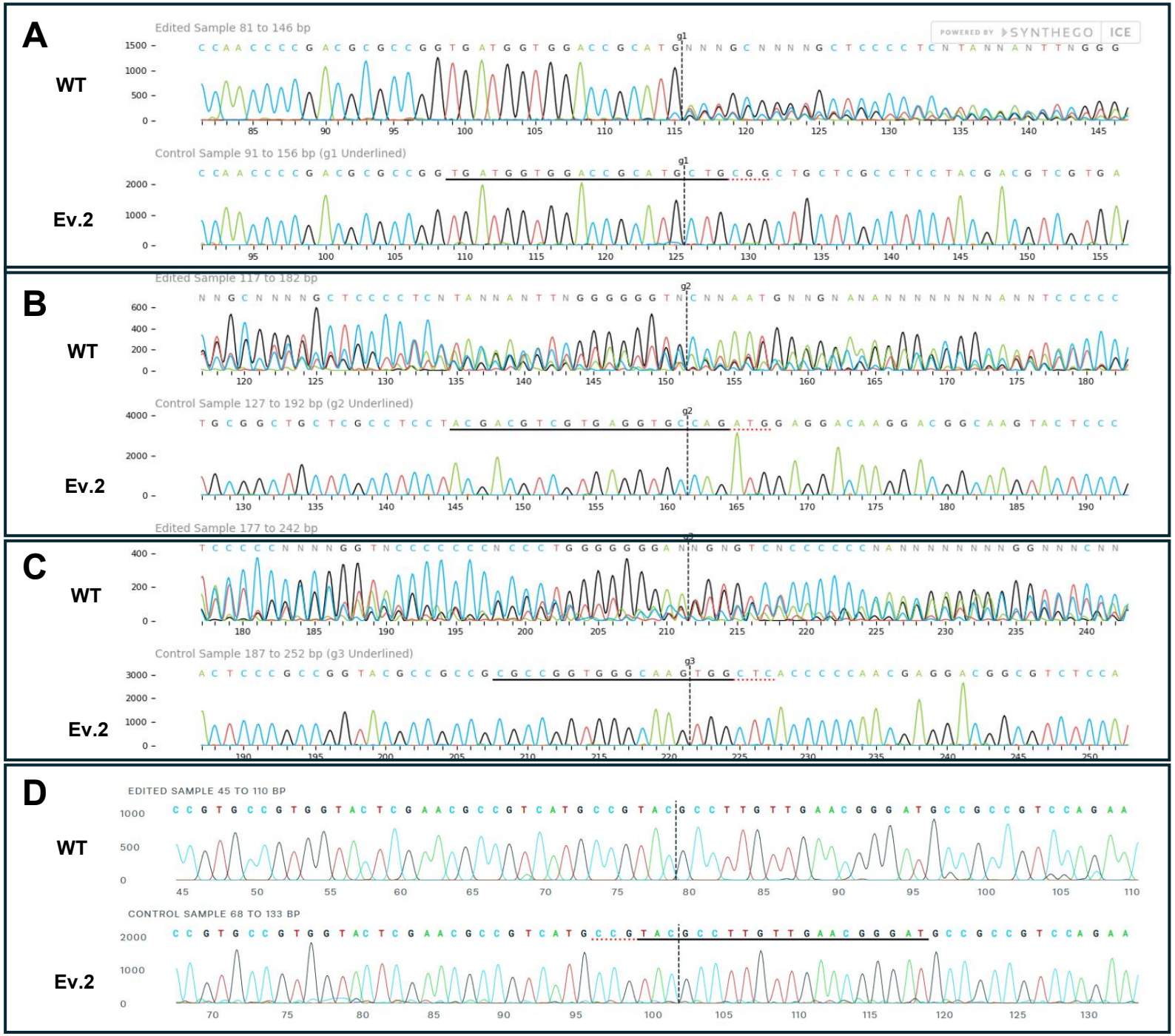
A
WT
Ev.2
Edited Sample 81 to 146 bp
Control Sample 91 to 156 bp (g1 Underlined)
g1
B
WT
Ev.2
Edited Sample 117 to 182 bp
Control Sample 127 to 192 bp (g2 Underlined)
g2
C
WT
Ev.2
Edited Sample 177 to 242 bp
Control Sample 187 to 252 bp (g3 Underlined)
g3
D
WT
Ev.2
EDITED SAMPLE 45 TO 110 BP
CONTROL SAMPLE 68 TO 133 BP

Figure S4

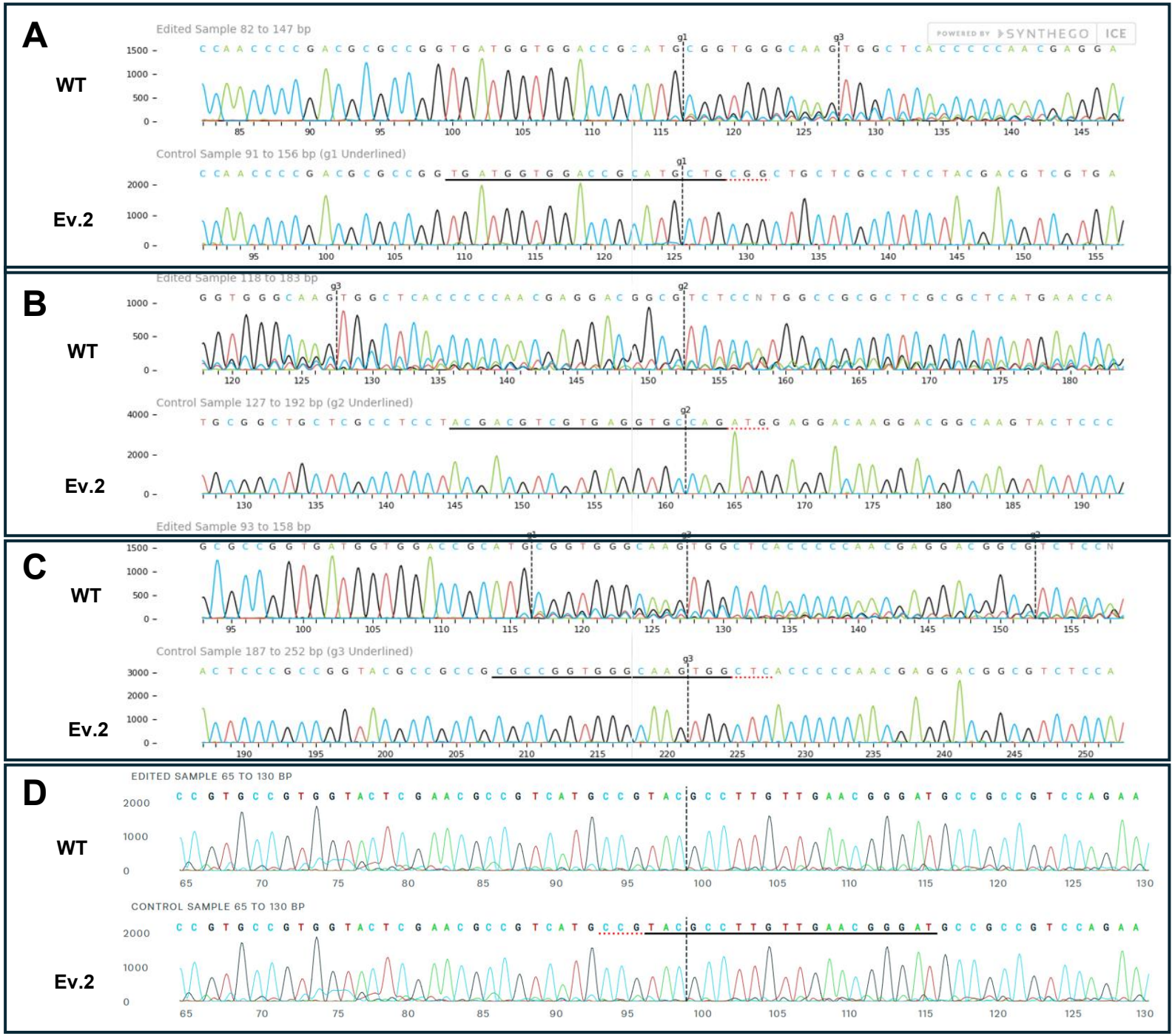
A
WT
Edited Sample 82 to 147 bp
POWERED BY SYNTHEGO ICE
Control Sample 91 to 156 bp (g1 Underlined)
Ev.2
B
WT
Edited Sample 118 to 183 bp
Control Sample 127 to 192 bp (g2 Underlined)
Ev.2
C
WT
Edited Sample 93 to 158 bp
Control Sample 187 to 252 bp (g3 Underlined)
Ev.2
D
WT
EDITED SAMPLE 65 TO 130 BP
CONTROL SAMPLE 65 TO 130 BP
Ev.2

Figure S5

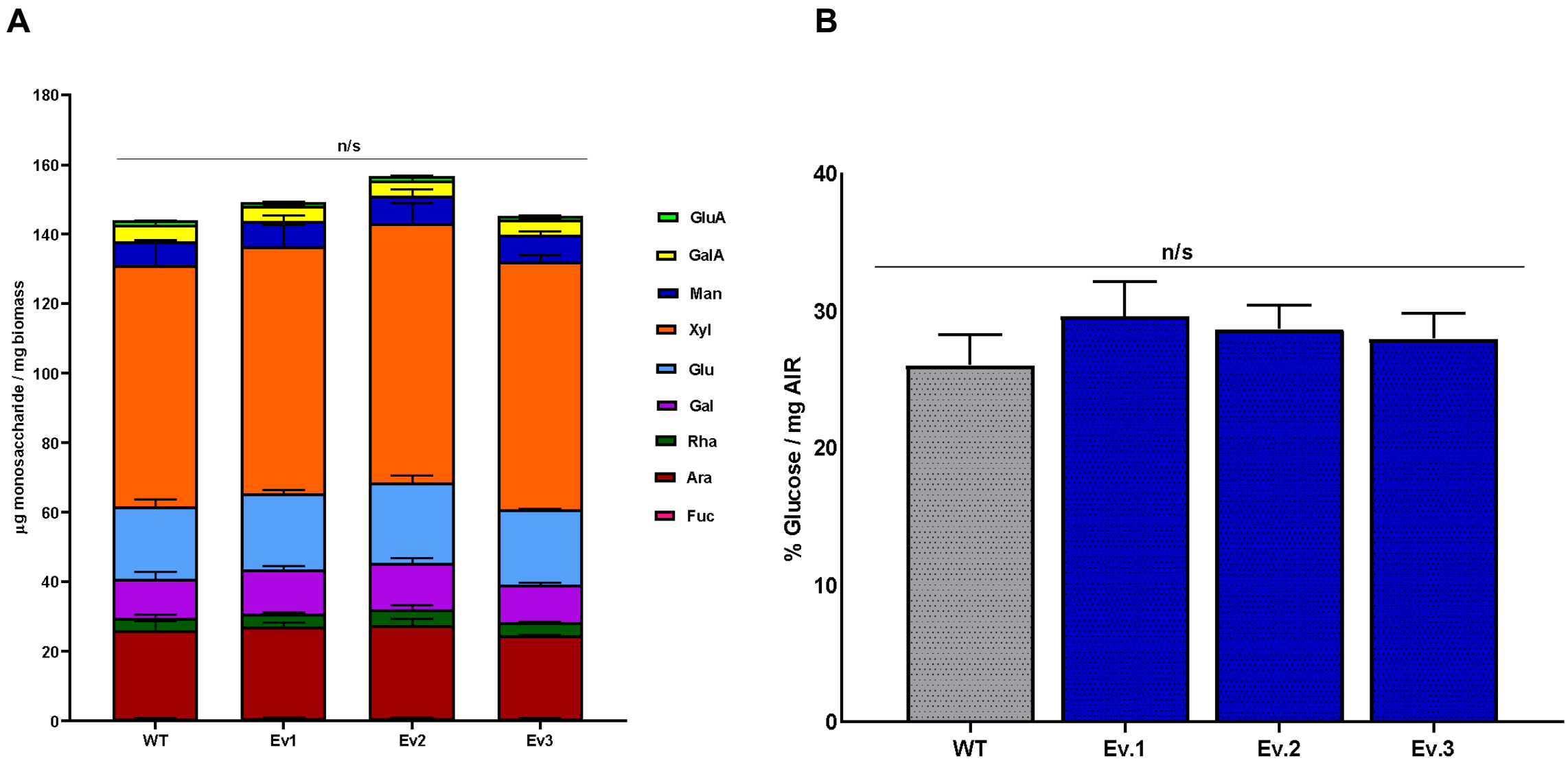
A
180
160
140
120
100
80
60
40
20
0
µg monosaccharide / mg biomass
n/s
WT
Ev1
Ev2
Ev3
GluA
GalA
Man
Xyl
Glu
Gal
Rha
Ara
Fuc
B
40
30
20
10
0
% Glucose / mg AIR
n/s
WT
Ev.1
Ev.2
Ev.3

Figure S6

A
5 cm
WT
Ev. 1
Ev. 2
Ev. 3
B
5 cm
WT
Ev. 1
Ev. 2
Ev. 3
C
5 cm
WT
Ev. 1
Ev. 2
Ev. 3

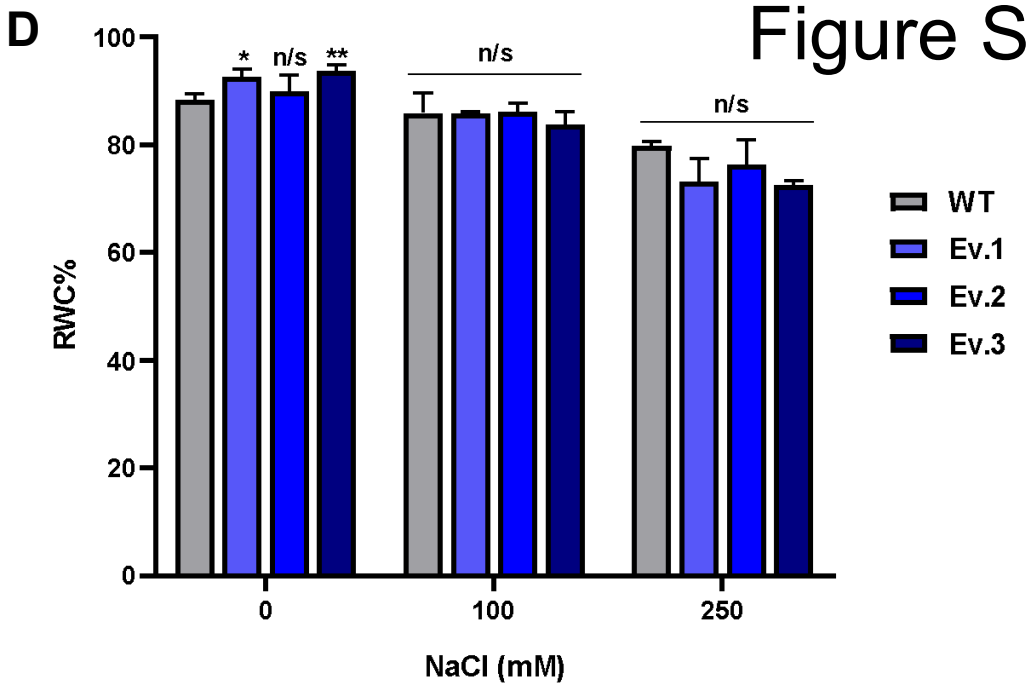
D
RWC%
100
80
60
40
20
0
*
n/s
**
n/s
n/s
0
100
250
NaCl (mM)
WT
Ev.1
Ev.2
Ev.3

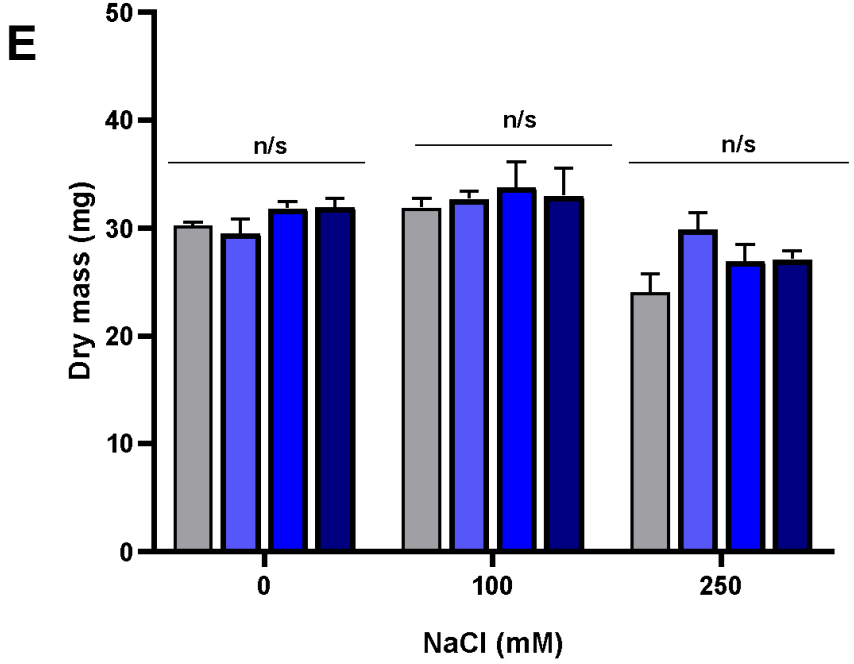
E
Dry mass (mg)
50
40
30
20
10
0
n/s
n/s
n/s
0
100
250
NaCl (mM)